Martian Moons eXploration (MMX)

JAXA's next-generation sample return mission

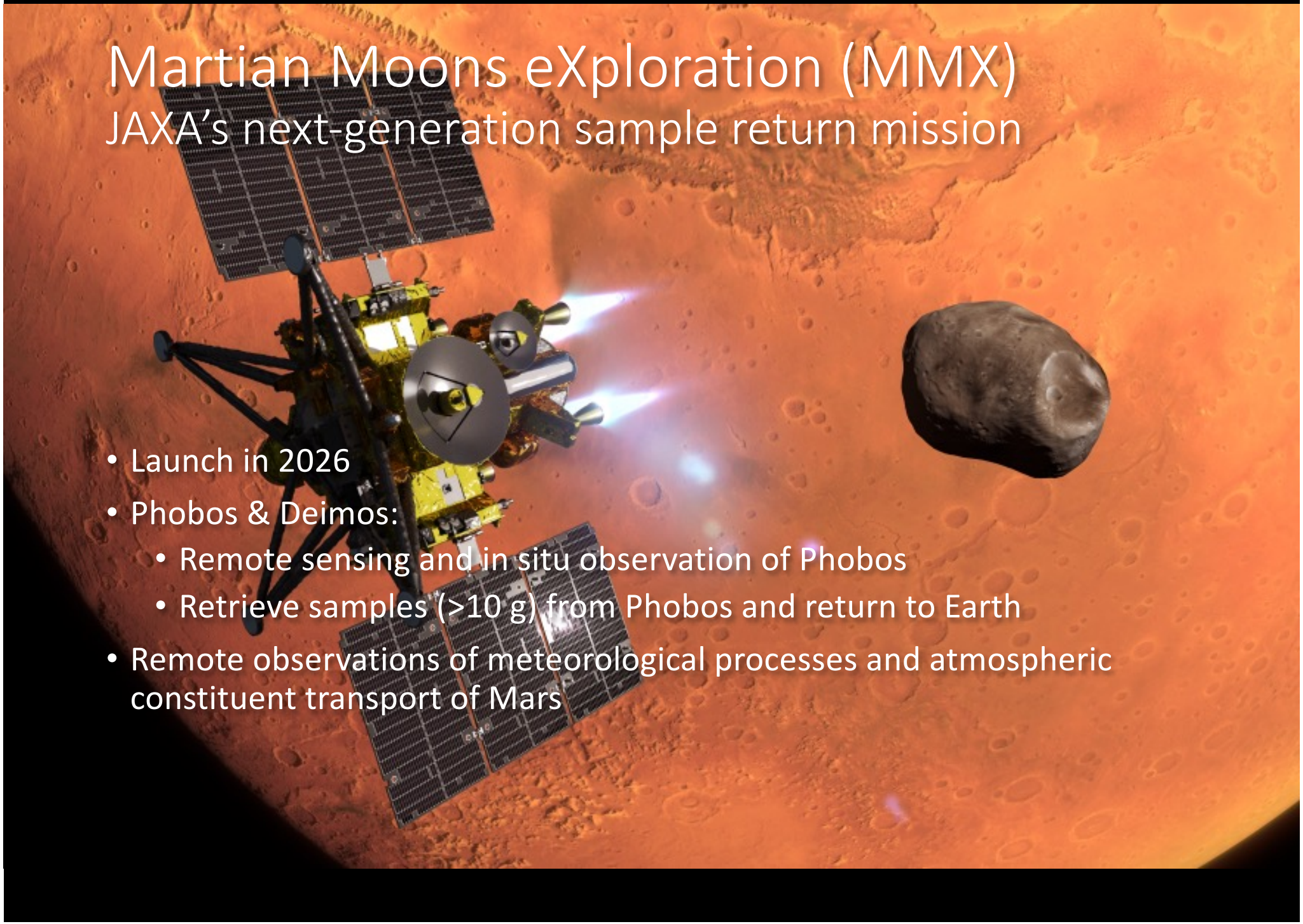

- Launch in 2026
- Phobos & Deimos:
  - Remote sensing and in situ observation of Phobos
  - Retrieve samples (>10 g) from Phobos and return to Earth
- Remote observations of meteorological processes and atmospheric constituent transport of Mars

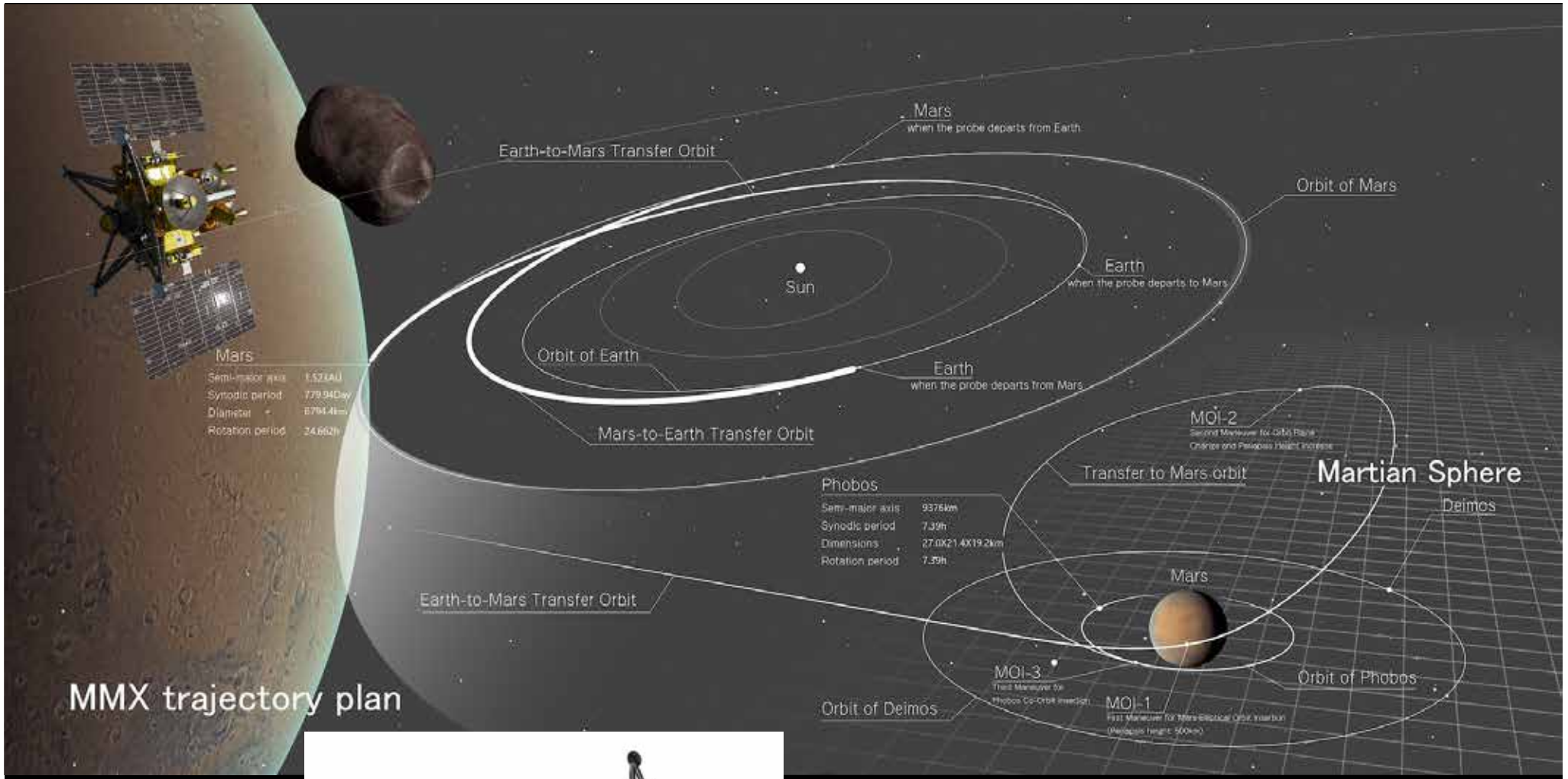
MMX trajectory plan
Mars
when the probe departs from Earth
Earth-to-Mars Transfer Orbit
Orbit of Mars
Sun
Earth
when the probe departs to Mars
Orbit of Earth
Earth
when the probe departs from Mars
Mars-to-Earth Transfer Orbit
Mars
Semi-major axis 1.523AU
Synodic period 779.94Day
Diameter 6794.4km
Rotation period 24.66Zh
MOI-2
Transfer to Mars orbit
Martian Sphere
Deimos
Phobos
Semi-major axis 9376km
Synodic period 7.39h
Dimensions 27.0X21.4X19.2km
Rotation period 7.39h
Earth-to-Mars Transfer Orbit
Mars
MOI-3
MOI-1
Orbit of Phobos
Orbit of Deimos

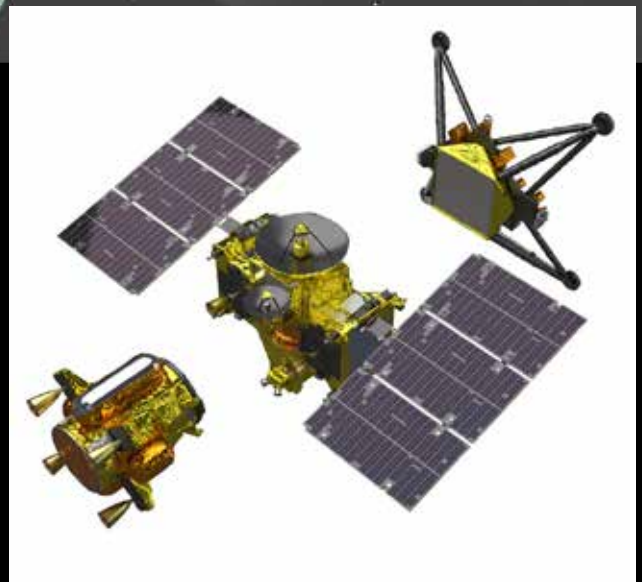

Instruments for Martian environment observation

- **OROCHI**
  - Wide-angle camera, 8 colors
  - 3 colors (480, 650, 950 nm) will be used for Mars observation.
  - 2.5 km/pix (sub S/C) from QSO
- **TENGOO**
  - Narrow-angle camera
  - 35 m/pix (sub S/C) from QSO
- **MIRS**
  - Push-bloom type spectrometer
  - Spectral resolution: 10nm
  - Spectral bandpass: 0.9–3.6 μm
  - 2.1 km/pix (sub S/C) from QSO
- **MSA**
  - In-situ observations of the escaping atmosphere with high mass resolution
  - M/dM > 100
  - H^+, O^+, C^+, N^+, $^{18}O^+$, $^{13}C^+$, …

TENGOO, OROCHI
Kameda et al. (2021)

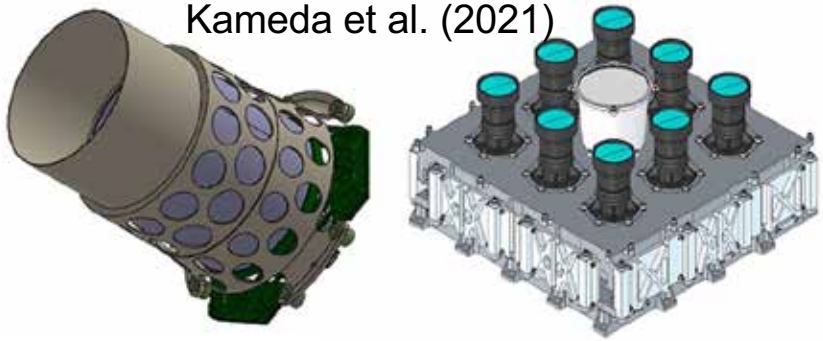

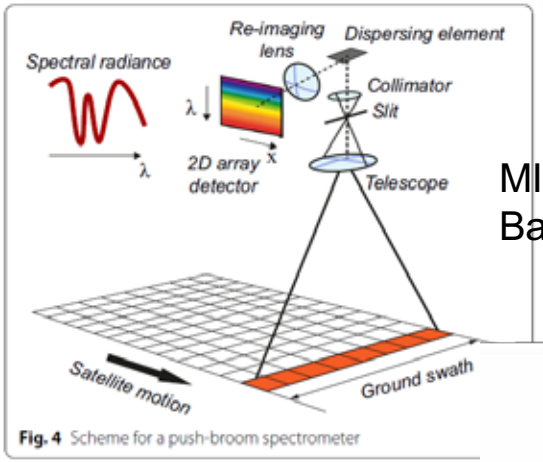

Fig. 4 Scheme for a push-broom spectrometer

MIRS
Barucci et al. (2021)

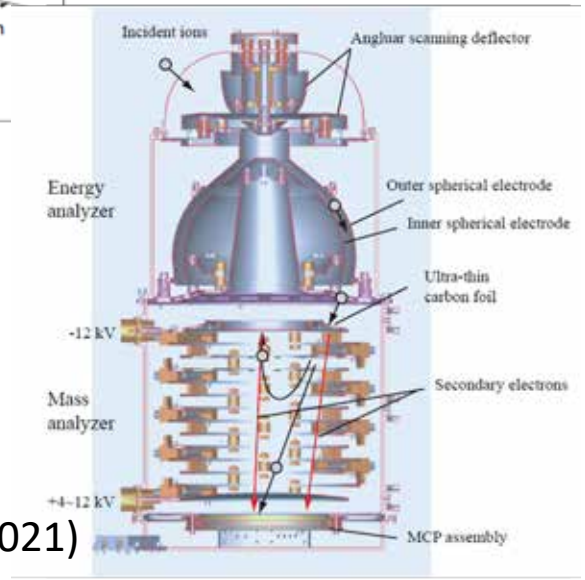

MSA
Yokota et al. (2021)

Continuous global monitoring from Martian orbit

Utilizing the high-altitude equatorial orbit as a unique platform for atmosphere studies

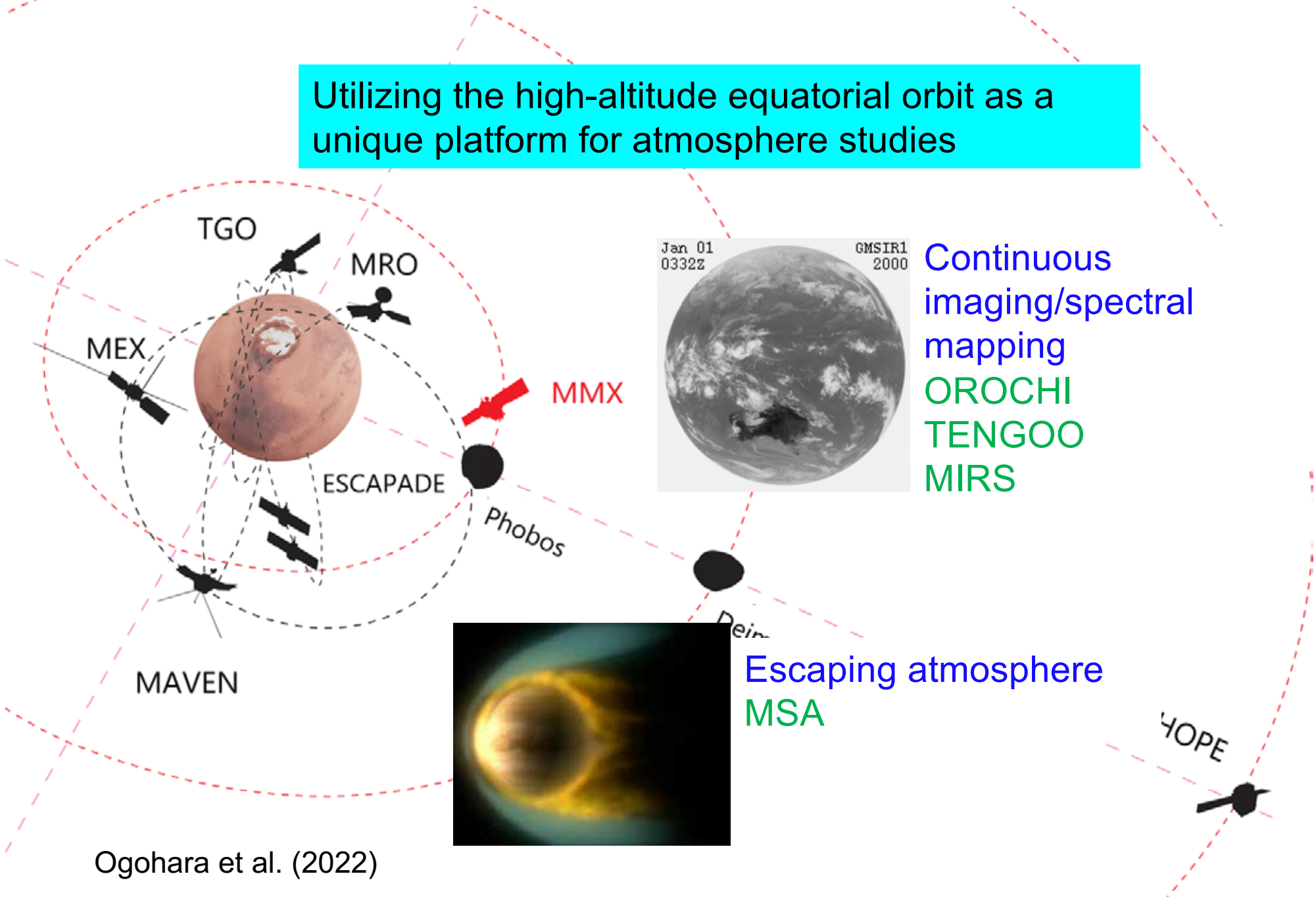

Continuous imaging/spectral mapping
OROCHI
TENGOO
MIRS

Escaping atmosphere
MSA

Ogohara et al. (2022)

Close coupling between the lower atmosphere and exosphere

Heavens et al. (2018)

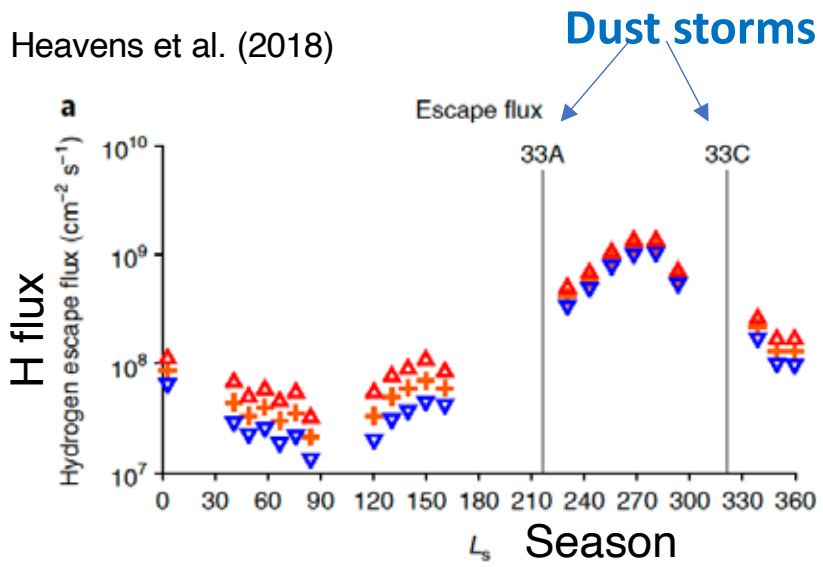

Hydrogen escape observed by MAVEN Solar Wind Ion Analyzer

➡ MSA

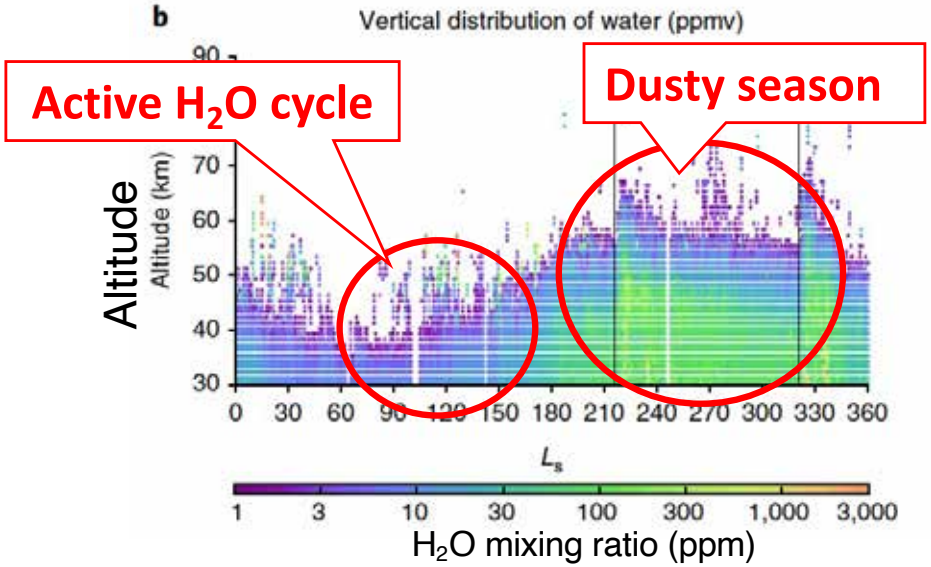

Vertical distribution of H_2O observed by Mars Reconnaissance Orbiter MCS

➡ OROCHI
TENGOO
MIRS

Different seasons will be covered

Climate variation

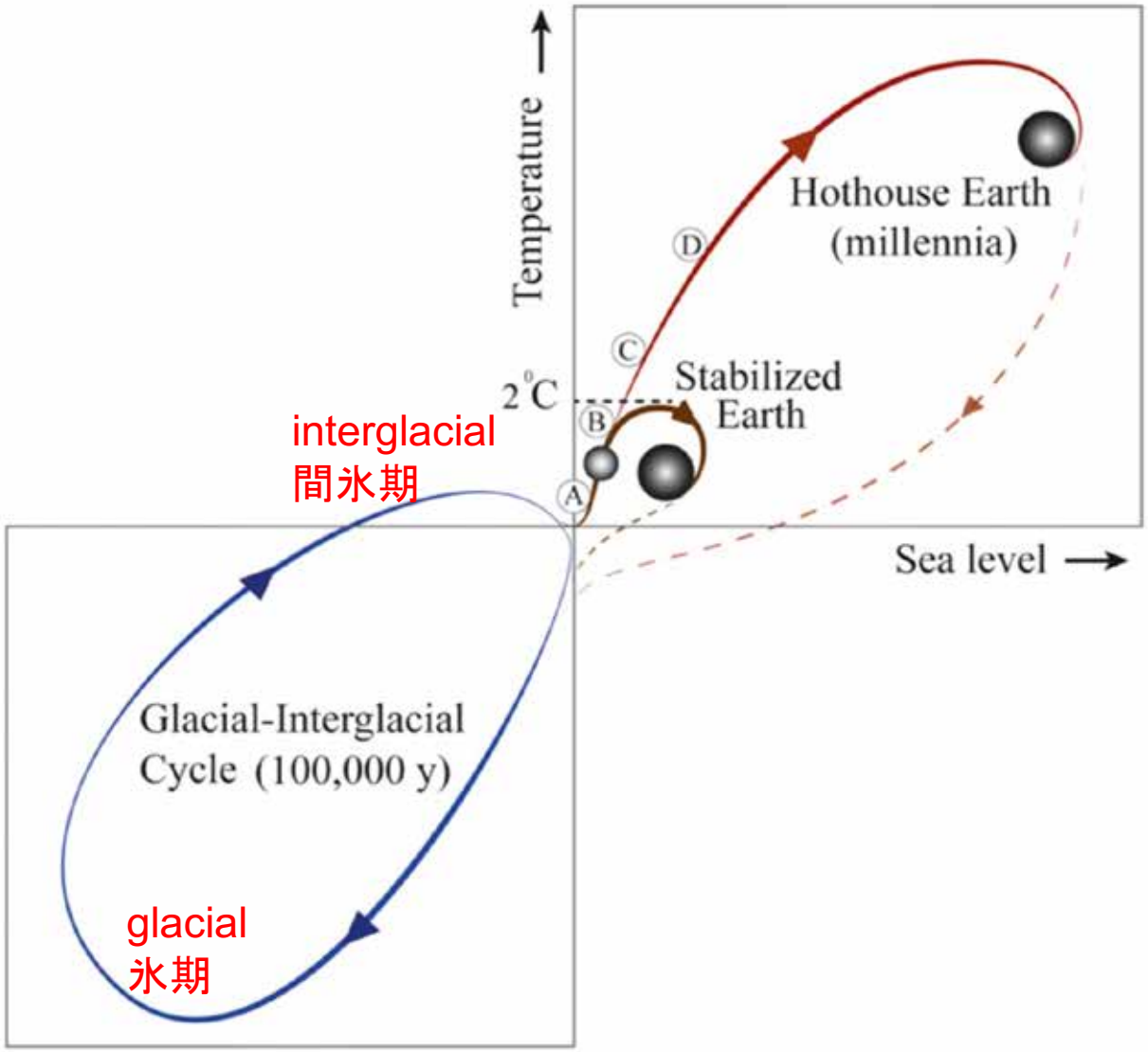

Steffen et al. (PNAS, 2018)

Milankovitch cycle

from Wikipedia

Precession 歳差

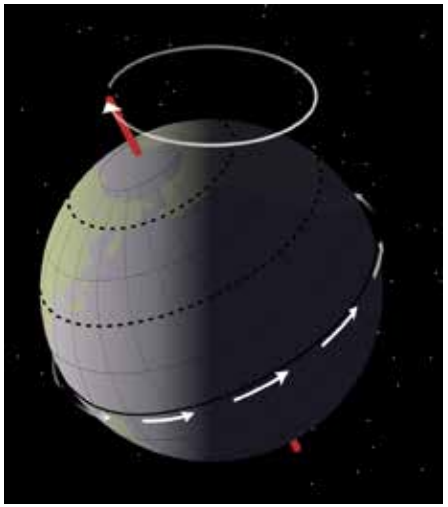

Obliquity 自転軸傾斜角

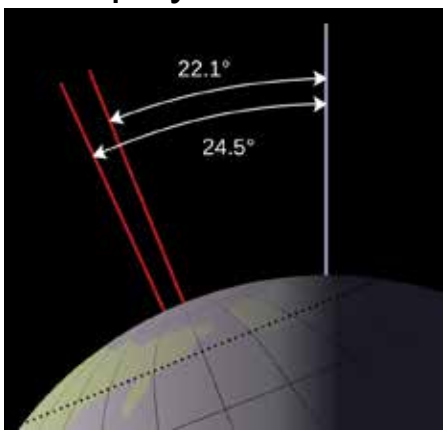

cold northern summer → growth of ice sheets
→ glacial inception (ice age)

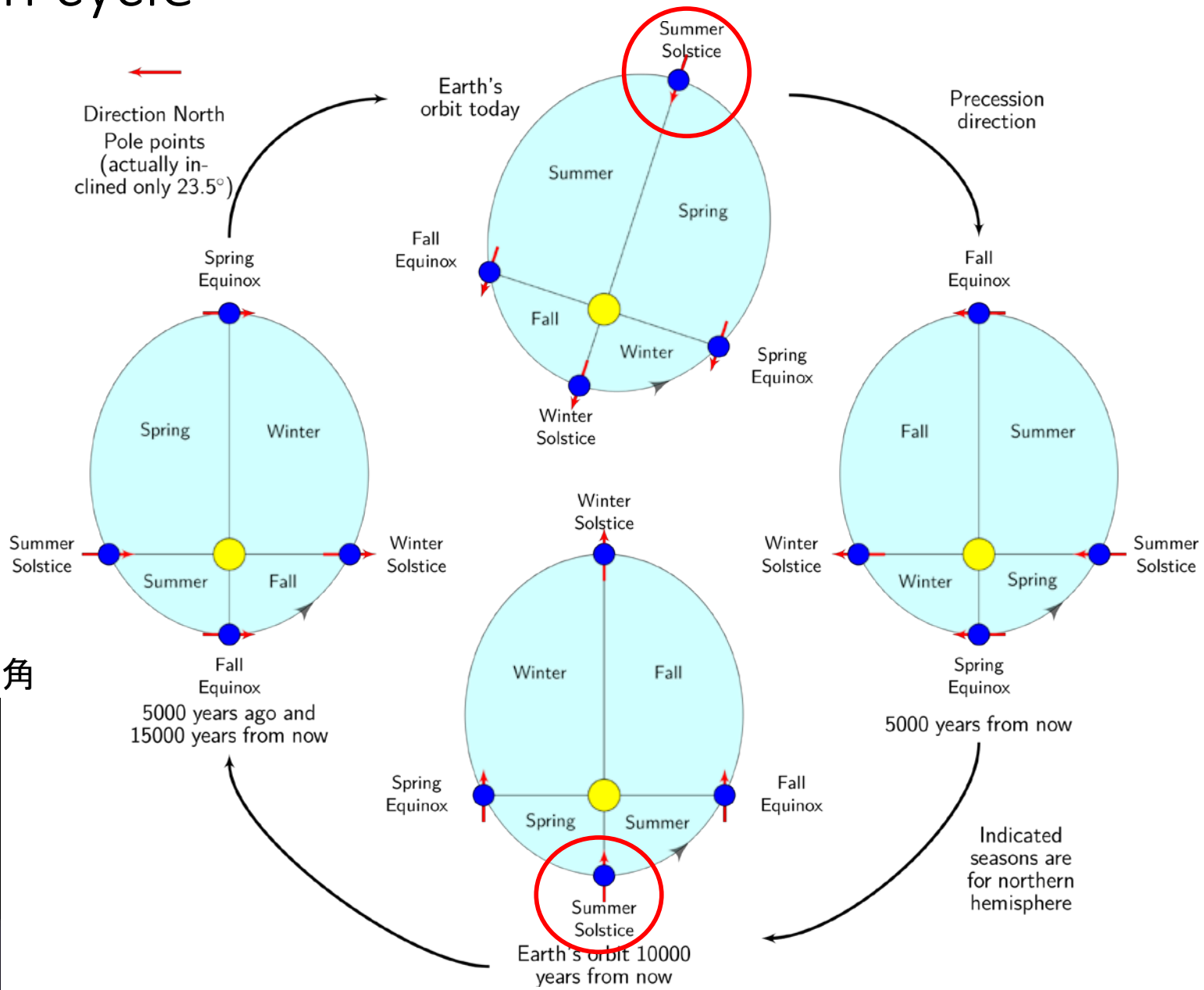

warm northern summer → decay of ice sheets
→ Interglacial (warm interval)

Milankovitch cycles on Mars and Earth

Table 12.10 The orbital elements of Mars and the Earth and their variability.

		Martian variability			Terrestrial variability	
Parameter	Present Mars	Range	Cycle (years)	Present Earth	Range	Cycle (years)
Obliquity (°)	25.19	0–85*	120 000**	23.45	22–24	41 000
Eccentricity	0.093	0–0.12	120 000***	0.017	0.01–0.04	100 000
Longitude of perihelion (°)	250	0–360	51 000	285	0–360	21 000

* Before ~10 Ma, obliquity variations are chaotic. While unpredictable at an exact time, statistically they would have varied between 0 and 85° (Laskar *et al.*, 2004; Touma and Wisdom, 1993).
** The amplitude of obliquity oscillation is modulated with a ~1.2 Myr period envelope.
*** The amplitude of eccentricity oscillation is modulated with a ~2.4 Myr period envelope.

Catling & Kasting 2017

(Earth's) glacial inception by CO_2 emission

Ganopolski et al. 2016, Nature

- Interglacials (間氷期) occur during periods of high summer insolation (日射) in the high latitudes of the Northern Hemisphere. (Milankovitch theory)
- In the past, a decrease in Northern Hemisphere insolation to below its present-day level always led to the end of interglacials and rapid growth of continental ice sheets.
- However, at present, although summer insolation at 65°N is close to its minimum, there is no evidence for the beginning of a new ice age.
- Glacial inceptions have occurred in the past under similar orbital configurations.

- The current interglacial would have ended if the CO_2 concentration had stayed at a level of about 240 ppm, as was the case at the end of MIS19 (800 kyr BP).
- During the late Holocene (完新世：現代含む) before the beginning of the industrial era, the CO_2 concentration was about 280 ppm, leading to escape from glacial inception. Pre-industrial land-use at least partly contributed to the high Holocene CO_2 level.
- If carbon emission continues, glacial inception is very unlikely within the next 100,000 years. Anthropogenic interference will make the initiation of the next ice age impossible.

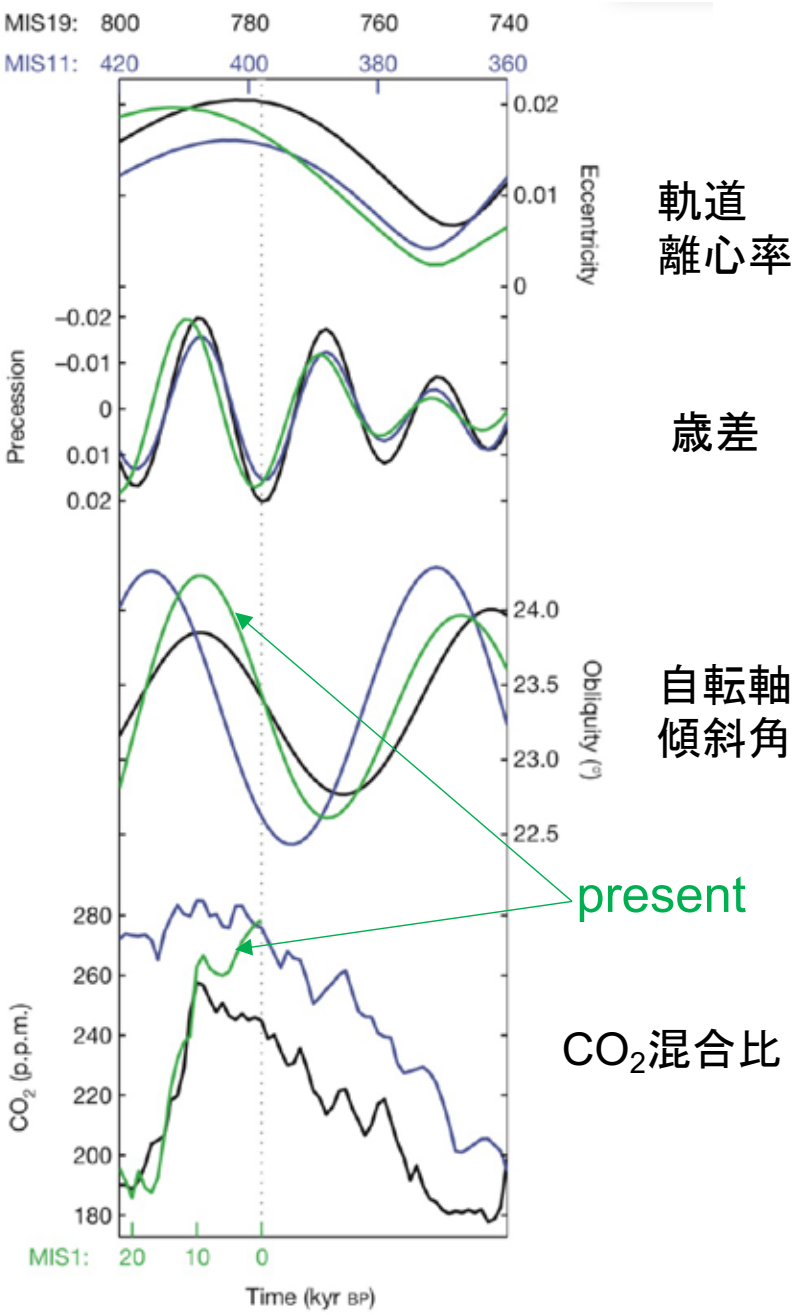

Ganopolski et al. 2016

Figure 1 | Orbital parameters. Comparison of Earth's orbital parameters and CO_2 concentrations for MIS1 (green), MIS11 (blue) and MIS19 (black). The vertical dashed line corresponds to the present day for MIS1 and the minima of the precessional component of insolation for MIS11 and MIS19.

Mars

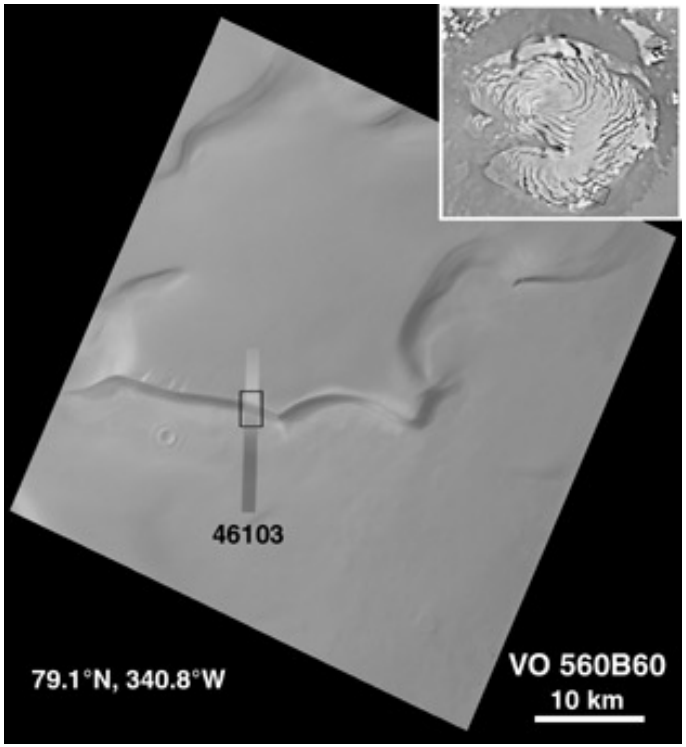

Polar cap deposits

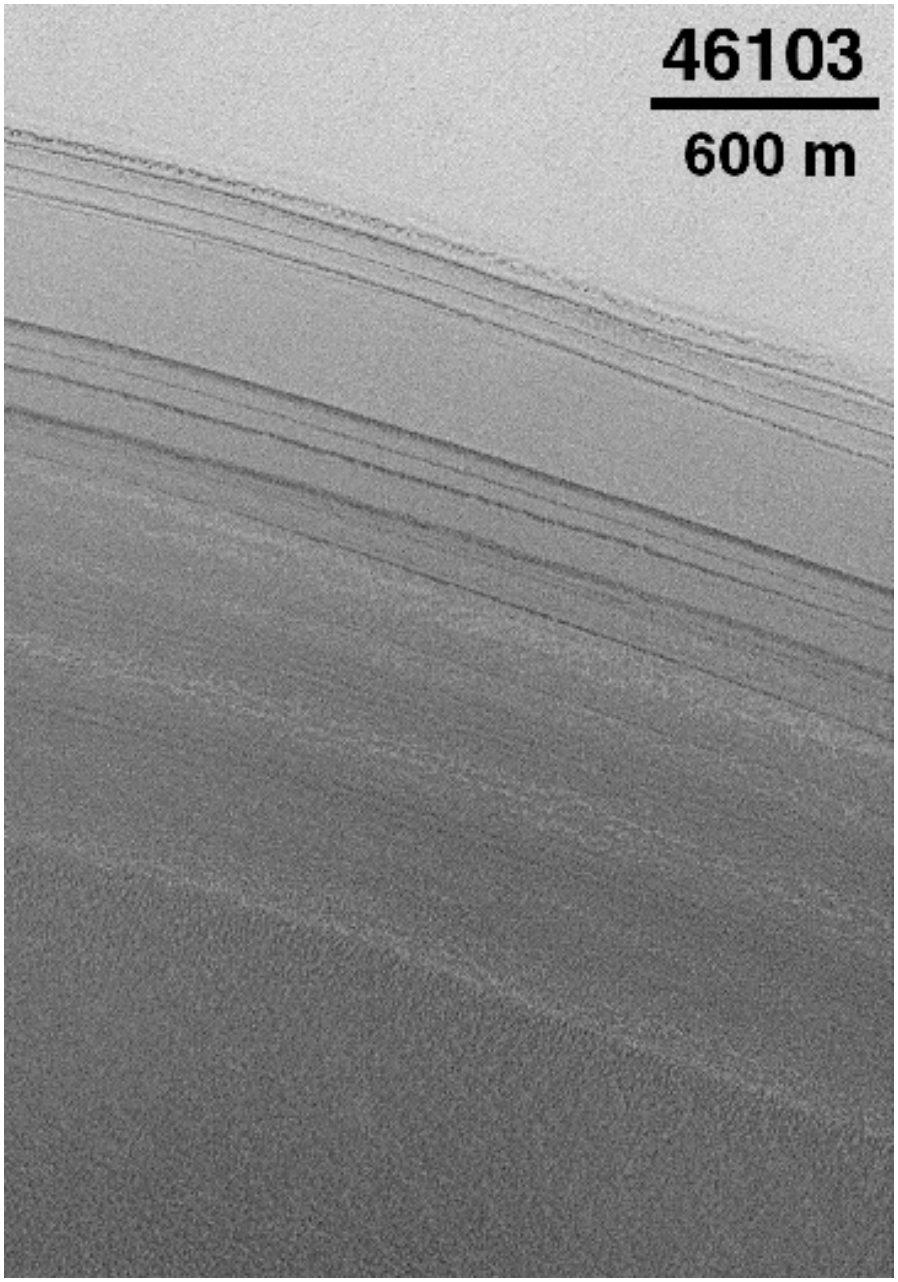

Recurrent slope lineae

Transition between different climate regimes ?

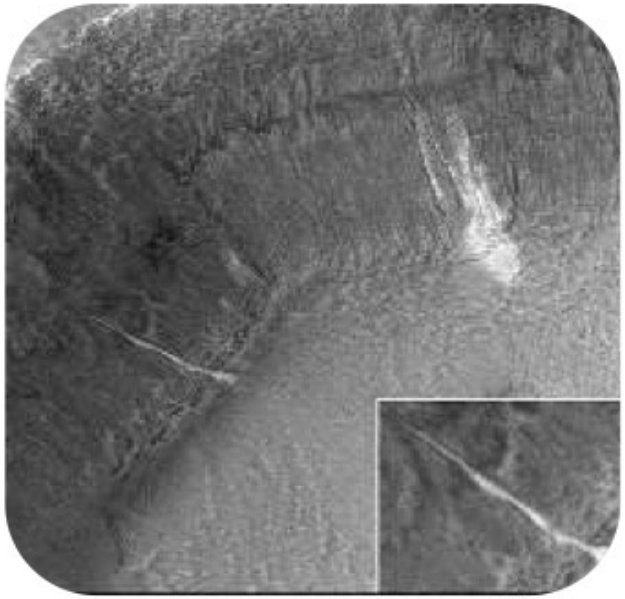

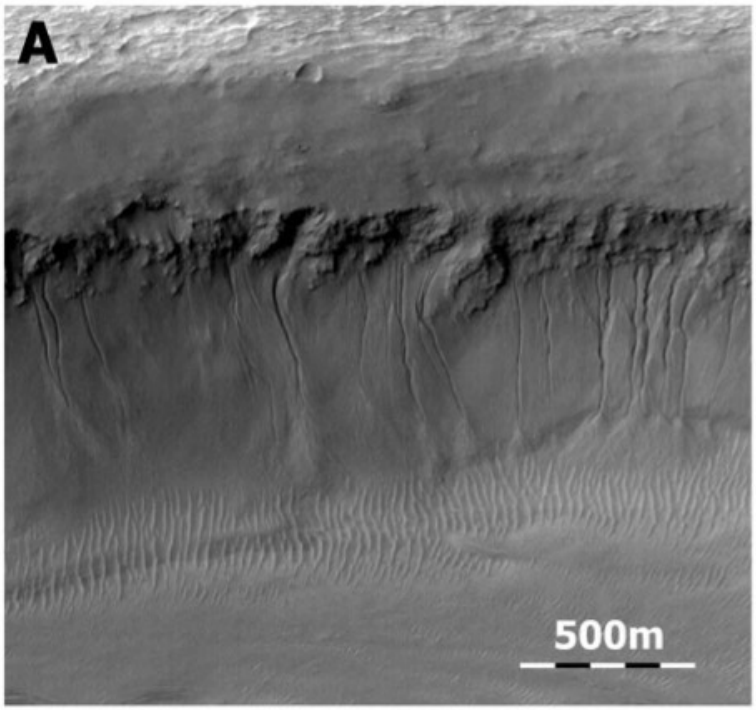

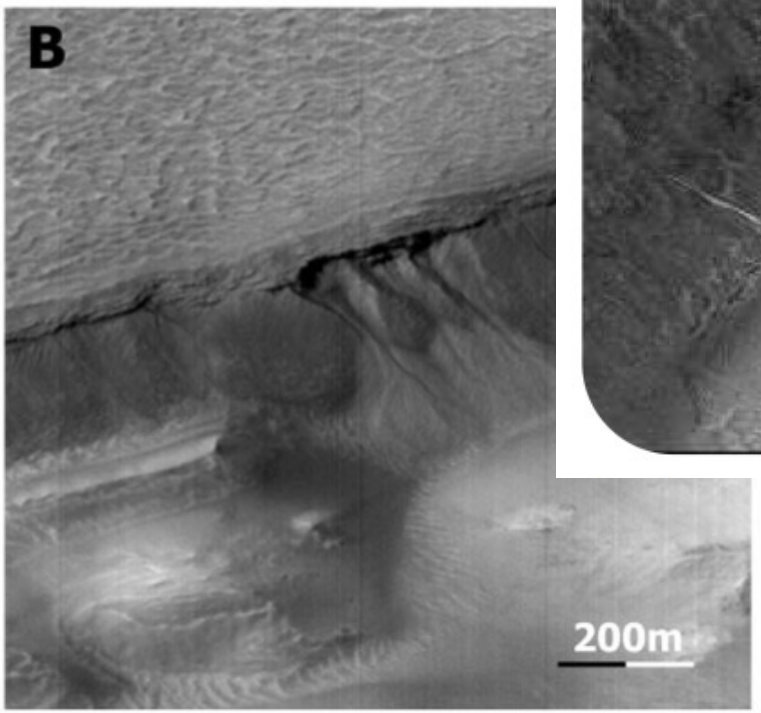

Subsurface ice

Mars Odyssey

Neutron Spectrometer (NS) and High-Energy Neutron Detector (HEND)

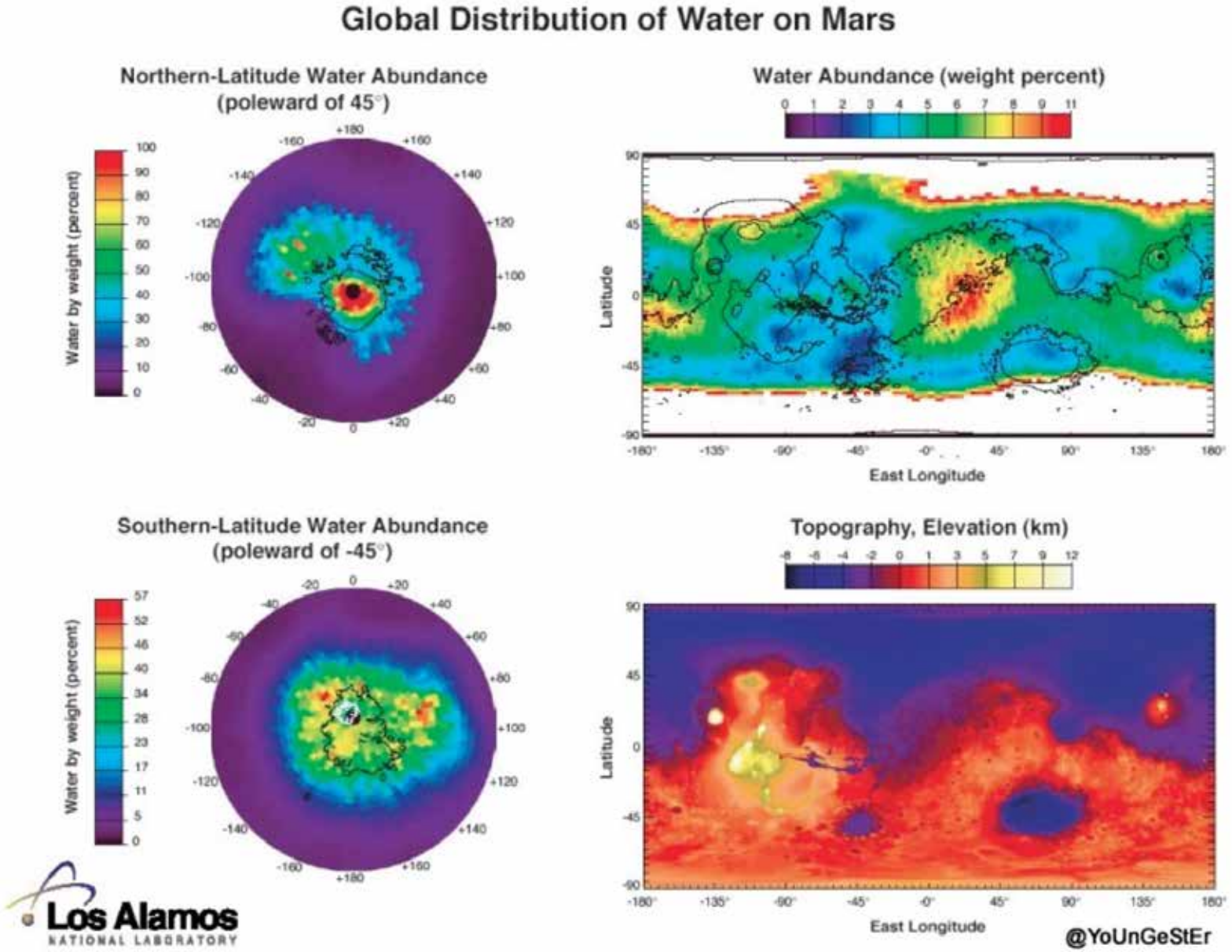

Schorghofer and Aharonson (2005)

Comparison with models

- Near equilibrium at high latitudes
- Non-equilibrium at low latitudes

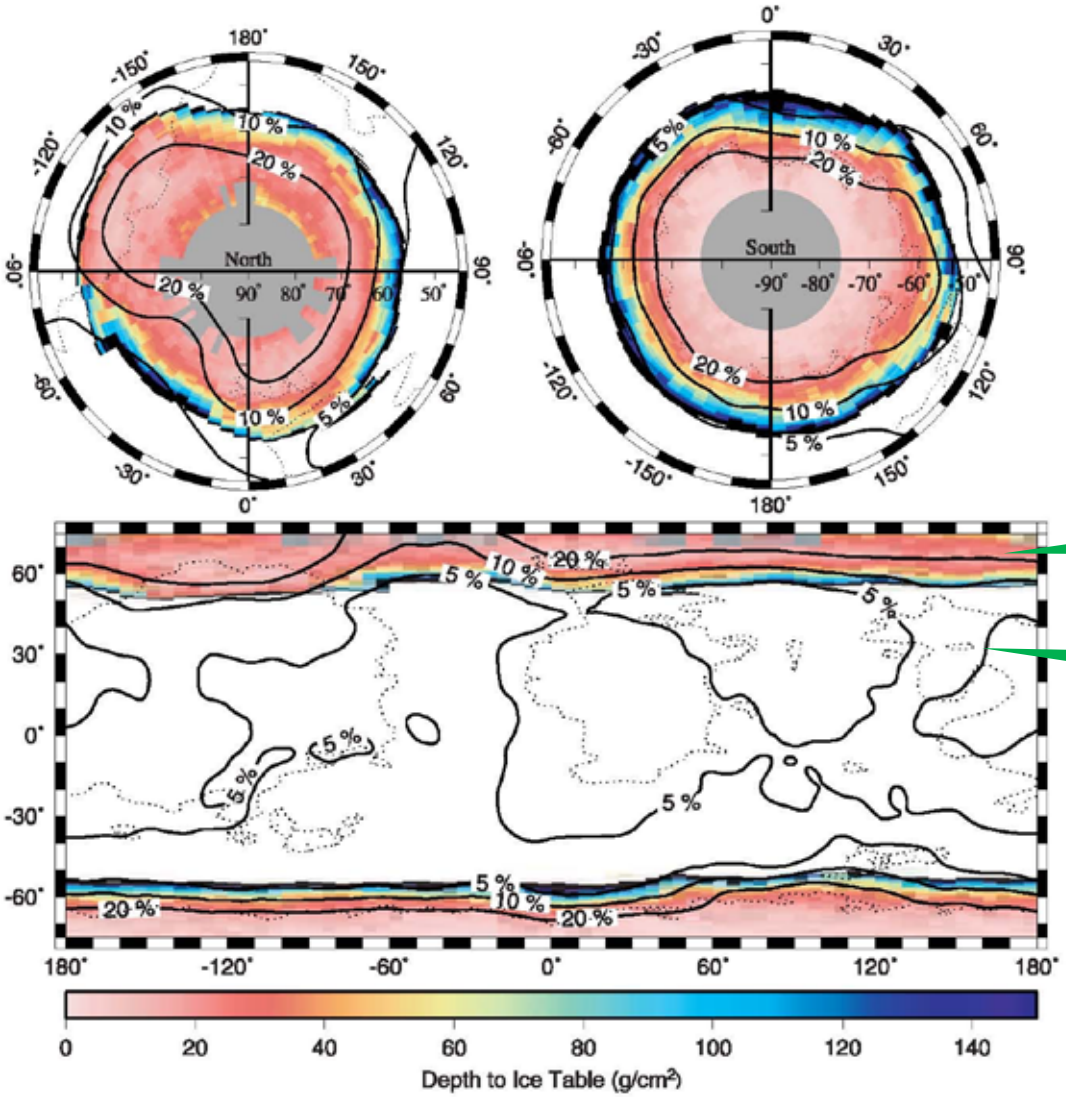

Figure 8. Color indicates depth to the ice table in g cm^{-2} when ice is in equilibrium with the atmospheric water vapor. Ground ice is unstable in the white area. Black segments indicate finite burial depths larger than 150 g cm^{-2}. Missing data points are shown in gray. Assumed volume fraction of ice is 40%, but the geographic boundary between icy and ice-free soil is independent of the ice fraction. Solid contours indicate water-equivalent hydrogen content in percent determined from neutron spectroscopy [*Feldman et al.*, 2004]. The dotted lines are 200 J $m^{-2}K^{-1}s^{-1/2}$ contours of thermal inertia.

Color: model prediction of H_2O ice sheets

Contour: observed H_2O

Buried glaciers

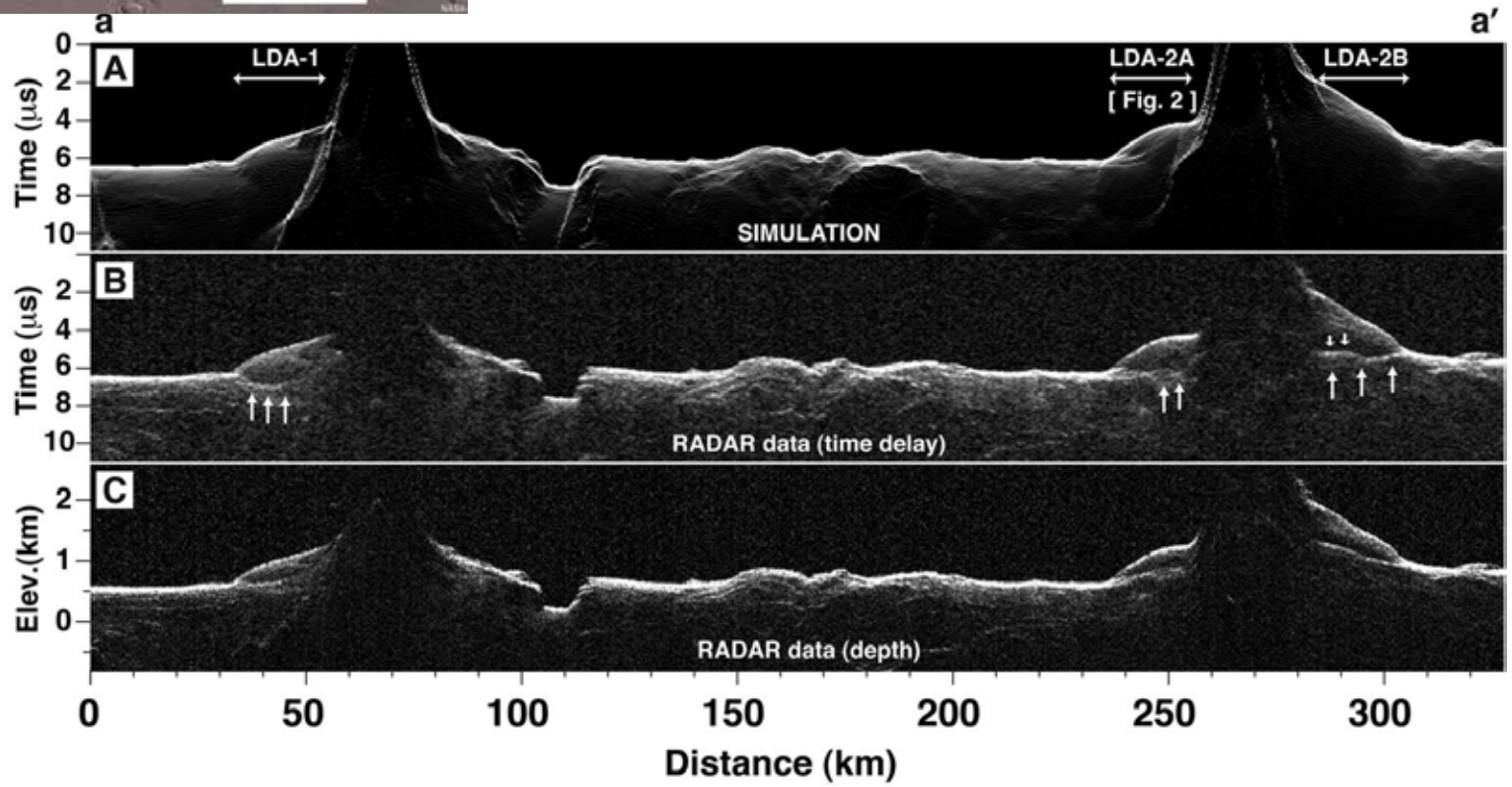

Milankovitch cycles on Mars and Earth

Table 12.10 The orbital elements of Mars and the Earth and their variability.

		Martian variability			Terrestrial variability	
Parameter	Present Mars	Range	Cycle (years)	Present Earth	Range	Cycle (years)
Obliquity (°)	25.19	0–85*	120 000**	23.45	22–24	41 000
Eccentricity	0.093	0–0.12	120 000***	0.017	0.01–0.04	100 000
Longitude of perihelion (°)	250	0–360	51 000	285	0–360	21 000

* Before ~10 Ma, obliquity variations are chaotic. While unpredictable at an exact time, statistically they would have varied between 0 and 85° (Laskar *et al.*, 2004; Touma and Wisdom, 1993).
** The amplitude of obliquity oscillation is modulated with a ~1.2 Myr period envelope.
*** The amplitude of eccentricity oscillation is modulated with a ~2.4 Myr period envelope.

Catling & Kasting 2017

Milankovitch cycles on Mars

自転軸傾斜角

軌道離心率

北極域の夏至の日射

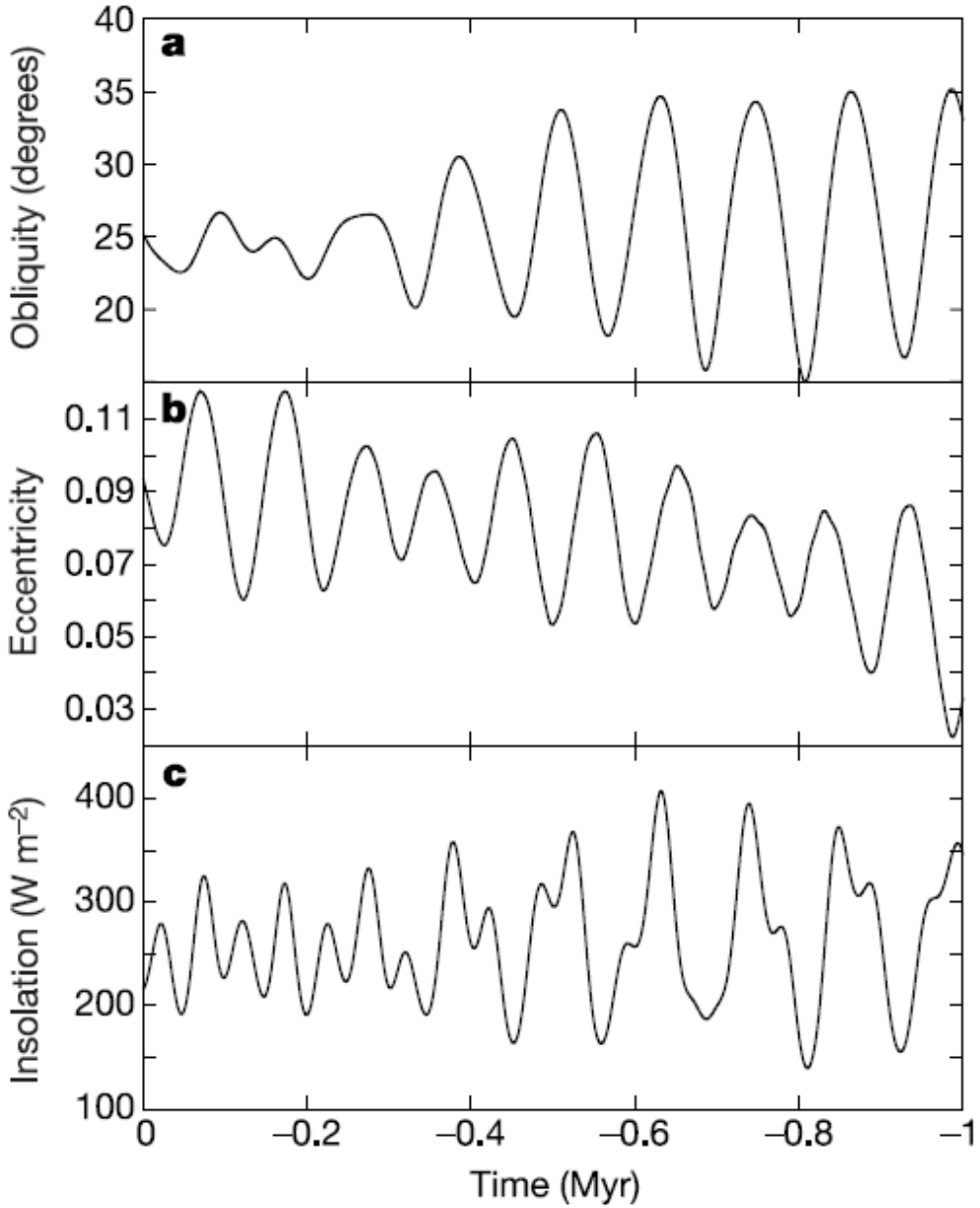

Laskar et al. (2002)

Seasons of Mars

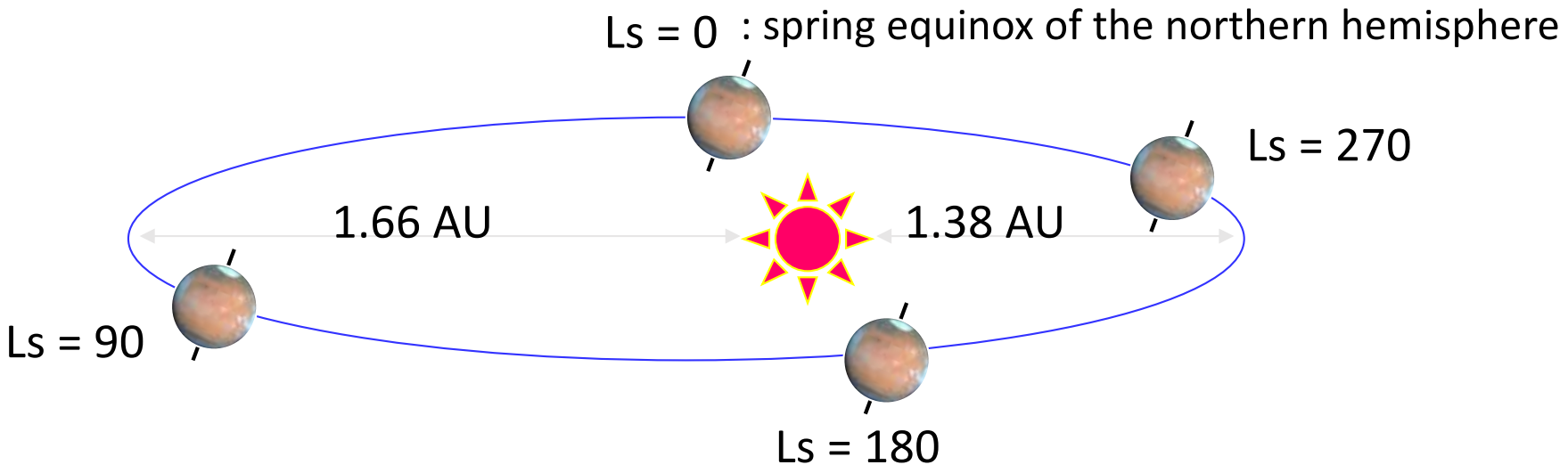

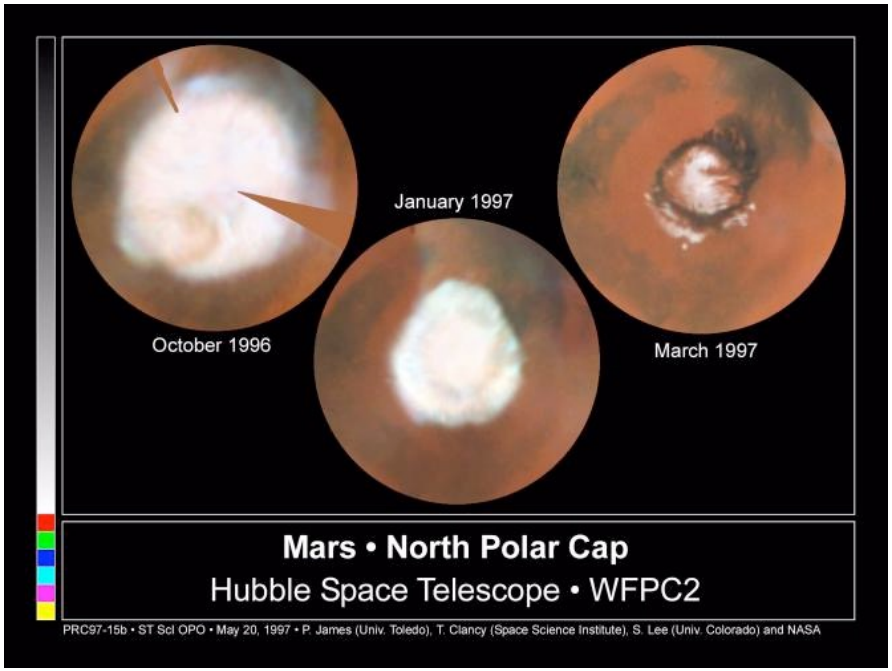

- 火星は公転軌道の離心率が大きいため季節変化が著しく南北非対称
- 南半球の夏に太陽までの距離が近くなる

Kieffer and Zent (Kieffer et al. eds, Univ. Arizona Press, 1992)

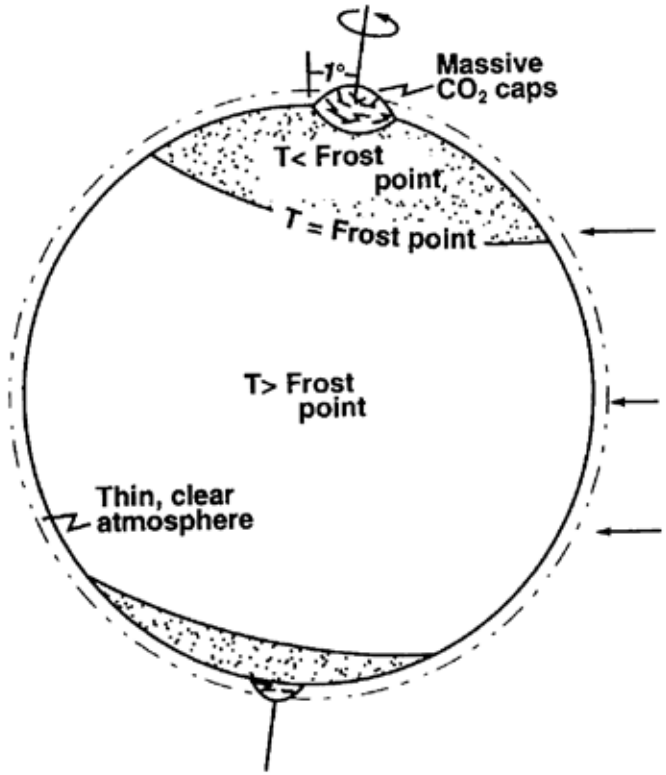

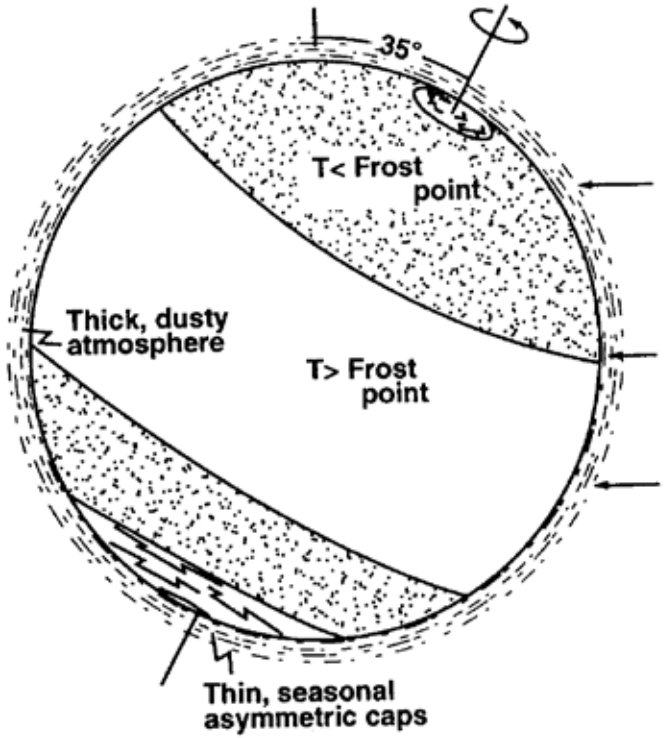

low obliquity → cold pole

→ massive polar cap

→ dry atmosphere

→ retreat of ice sheet

high obliquity → warm pole

→ thin polar cap

→ moist atmosphere

→ growth of ice sheet, ice accumulation in the tropics

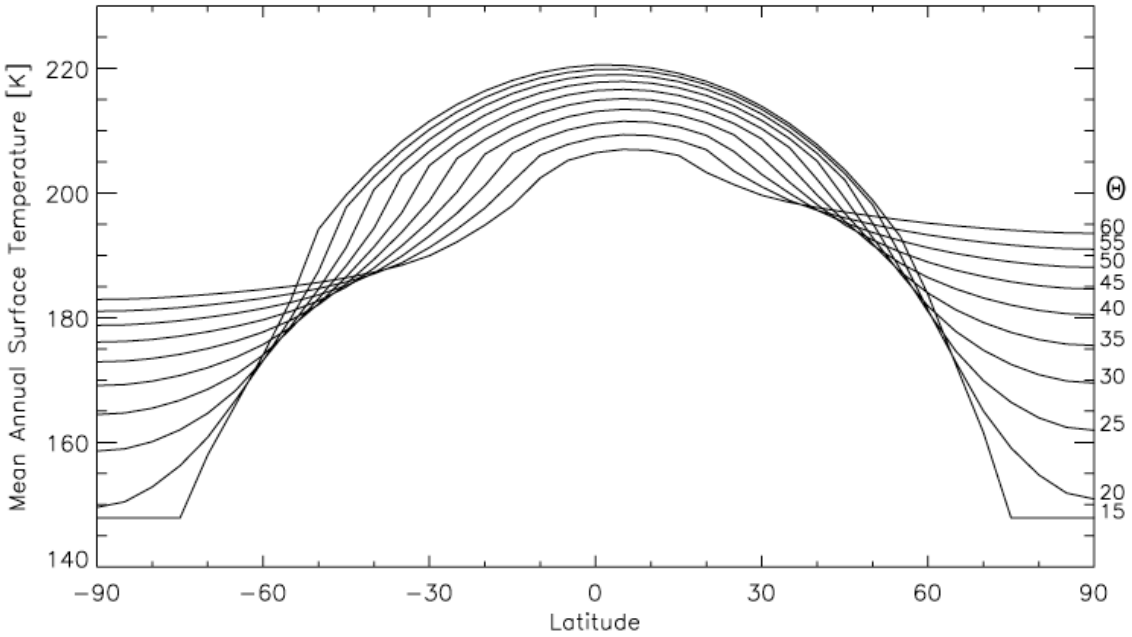

Figure 3. Mean annual surface temperature for a range of obliquities. The eccentricity is 0.12, and the L_S at which perihelion occurs is 270, corresponding to southern summer. A thermal inertia of 250 J m^{-2} s$^{-1/2}$ K^{-1}, an albedo of 0.25, a surface pressure of 600 Pa, and an infrared dust opacity of 0.1 are assumed. Discontinuities in the slope of each curve are due to the effects of seasonal CO_2 frost.

Mellon & Phillips (2001)

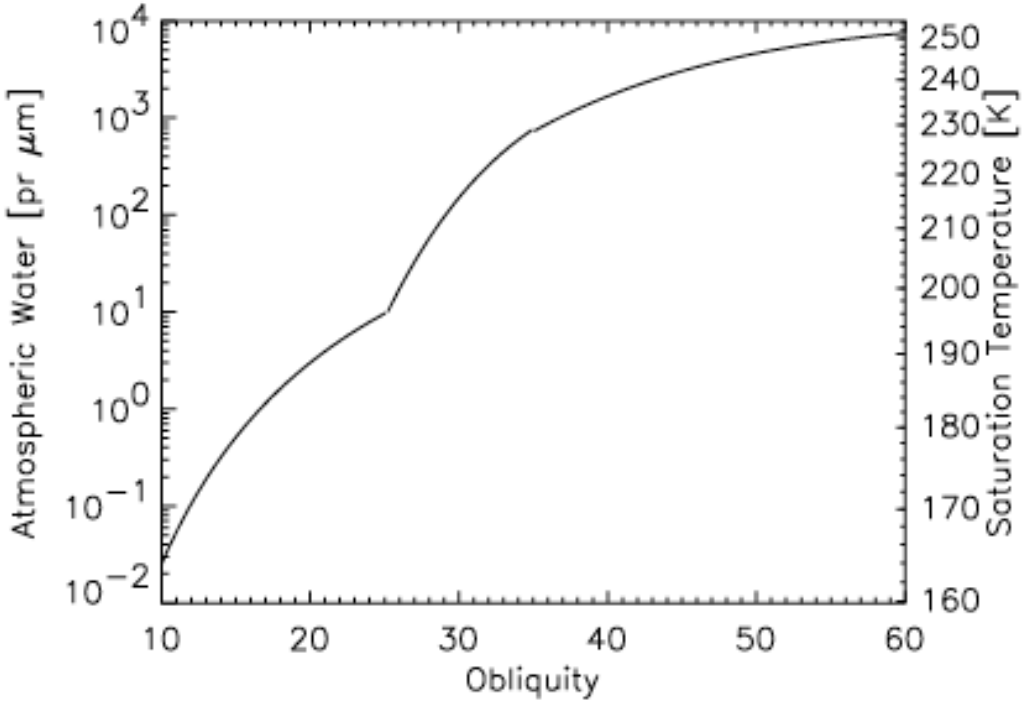

Formation of glaciers on Mars by atmospheric precipitation at high obliquity Forget et al. (2006)

- The model predicts ice accumulation in regions where glacier landforms are observed, on the western flanks of the great volcanoes and in the eastern Hellas region

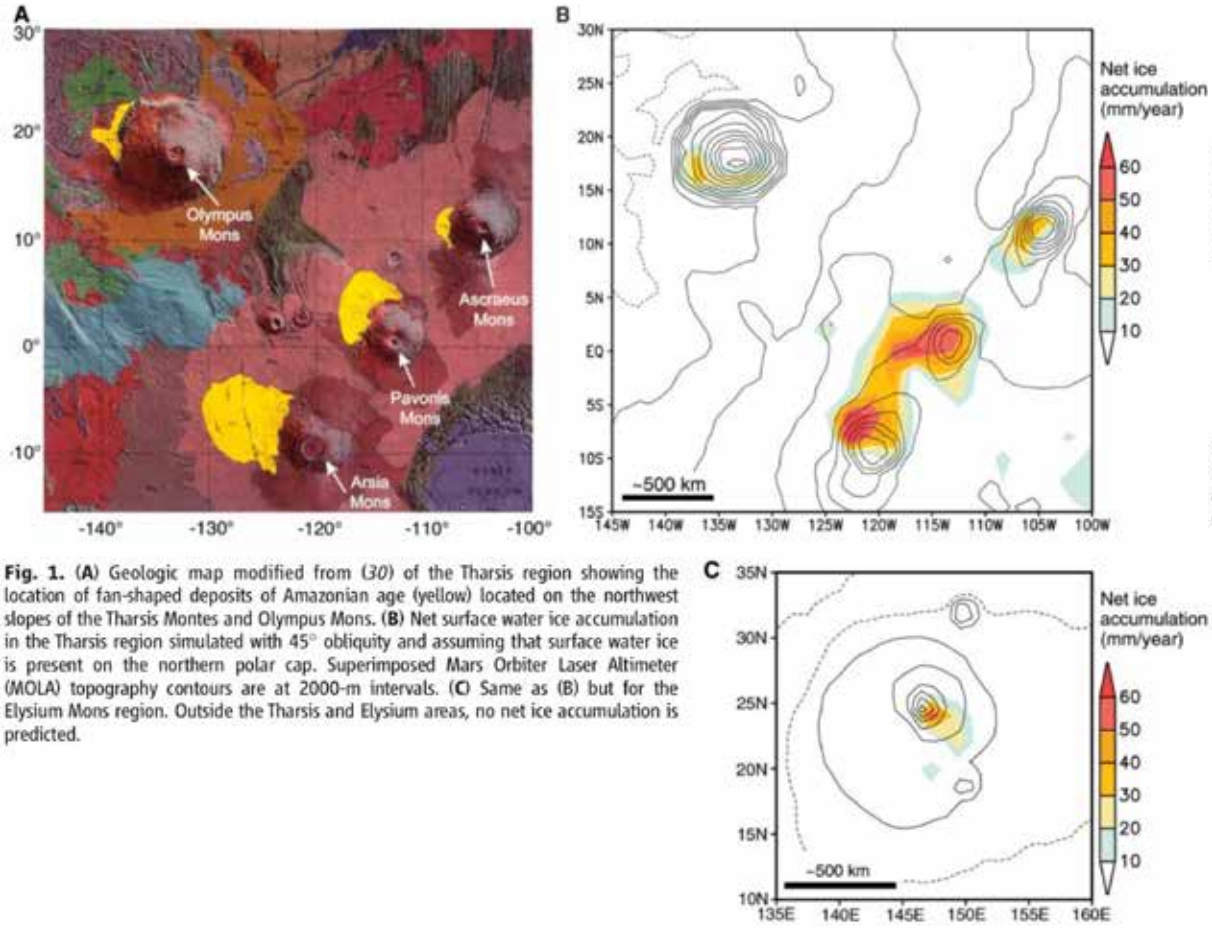

Fig. 1. (**A**) Geologic map modified from (*30*) of the Tharsis region showing the location of fan-shaped deposits of Amazonian age (yellow) located on the northwest slopes of the Tharsis Montes and Olympus Mons. (**B**) Net surface water ice accumulation in the Tharsis region simulated with 45° obliquity and assuming that surface water ice is present on the northern polar cap. Superimposed Mars Orbiter Laser Altimeter (MOLA) topography contours are at 2000-m intervals. (**C**) Same as (B) but for the Elysium Mons region. Outside the Tharsis and Elysium areas, no net ice accumulation is predicted.

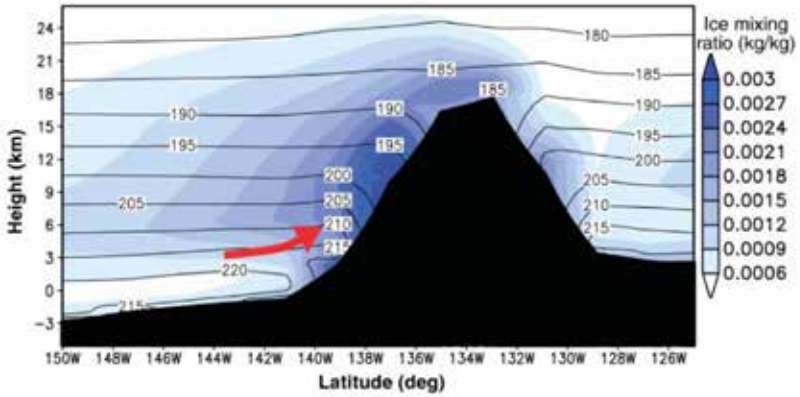

Fig. 3. Cross section of Olympus Mons along the 16°N latitude showing the mean atmospheric ice mass mixing ratio (shaded blue) and the atmospheric temperature (contour, K) averaged over the period of ice accumulation Ls = 125° to 155° (northern summer). The strong northwesterly winds induce adiabatic cooling on the flank of the volcanoes and atmospheric condensation and precipitation.

H_2SO_4 clouds of Venus

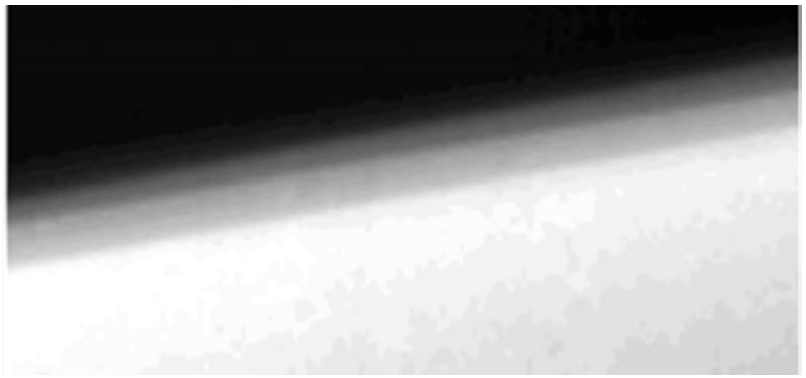

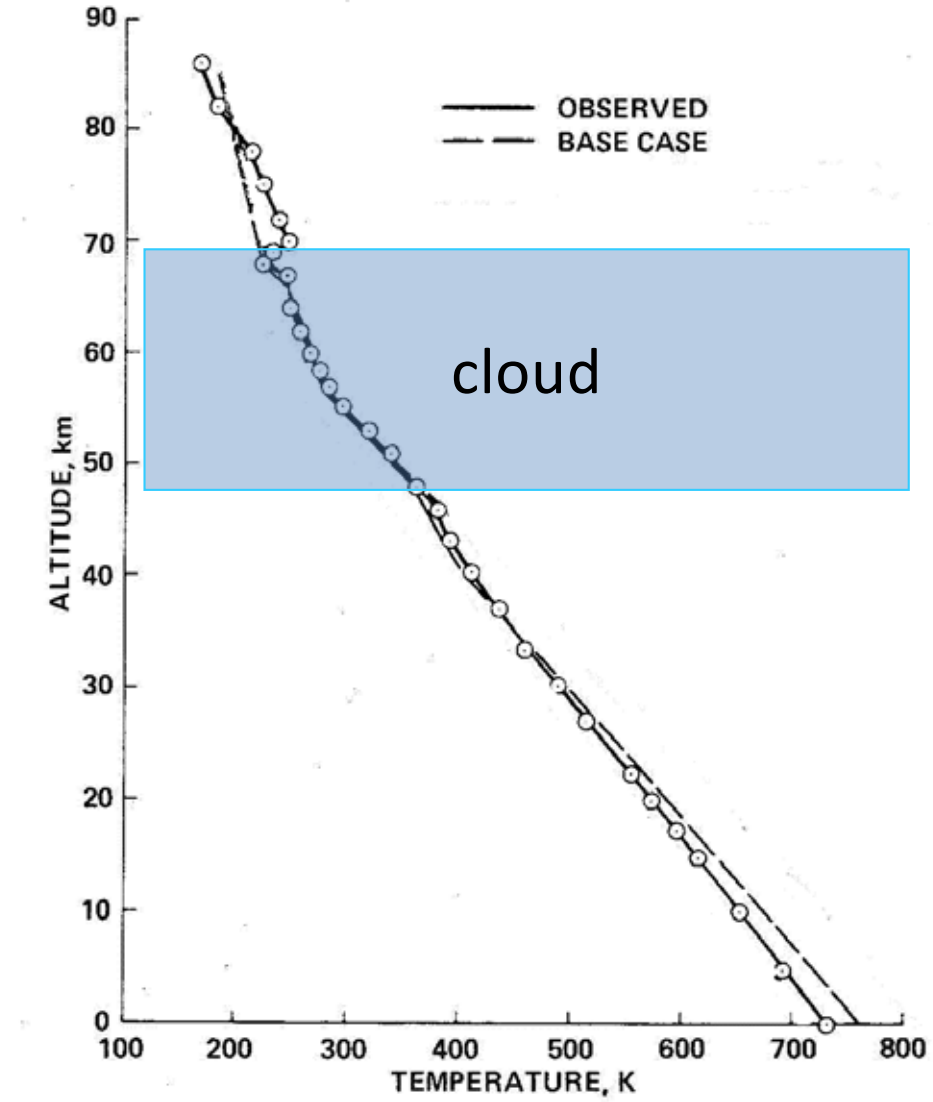

Fig. 2. Comparison between the observed temperature structure of Venus' lower atmosphere and that of several models, which are described in the main text.

- Solar energy flux reaching the Venus surface (17W/m^2) is much less than that of the Earth (168W/m^2).
- Greenhouse effect of massive CO_2 and small amount of H_2O explains the high temperature.

Pollack et al. (1980)

Origin of clouds

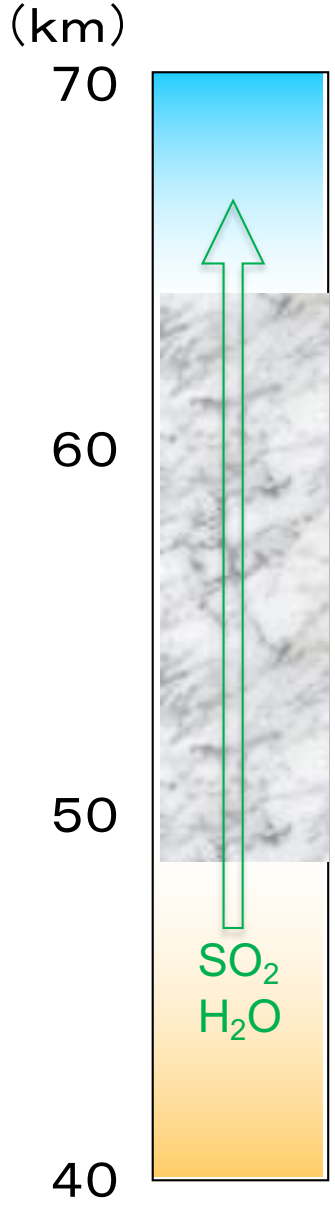

Photochemistry above clouds

Scenario #1 (Net reaction driven by catalytic cycles including ClOx, HOx, NOx)

$$2CO_2 + h\nu \rightarrow 2CO + O_2$$

$$CO + SO_2 + O_2 + h\nu \rightarrow CO_2 + SO_3$$

$$CO_2 + SO_2 + h\nu \rightarrow CO + SO_3$$

Scenario #2

$$SO_2 + h\nu \rightarrow SO + O$$

$$SO + h\nu \rightarrow S + O$$

$$SO_2 + O \rightarrow SO_3 \quad (\times 2)$$

$$3\,SO_2 + h\nu \rightarrow S + 2SO_3$$

- SO_3 rapidly reacts with H_2O: $SO_3 + H_2O \rightarrow H_2SO_4$
- Elemental sulfur (S) can serve as condensation nuclei.

Venus:

Massive eruptions several hundred million years ago ?

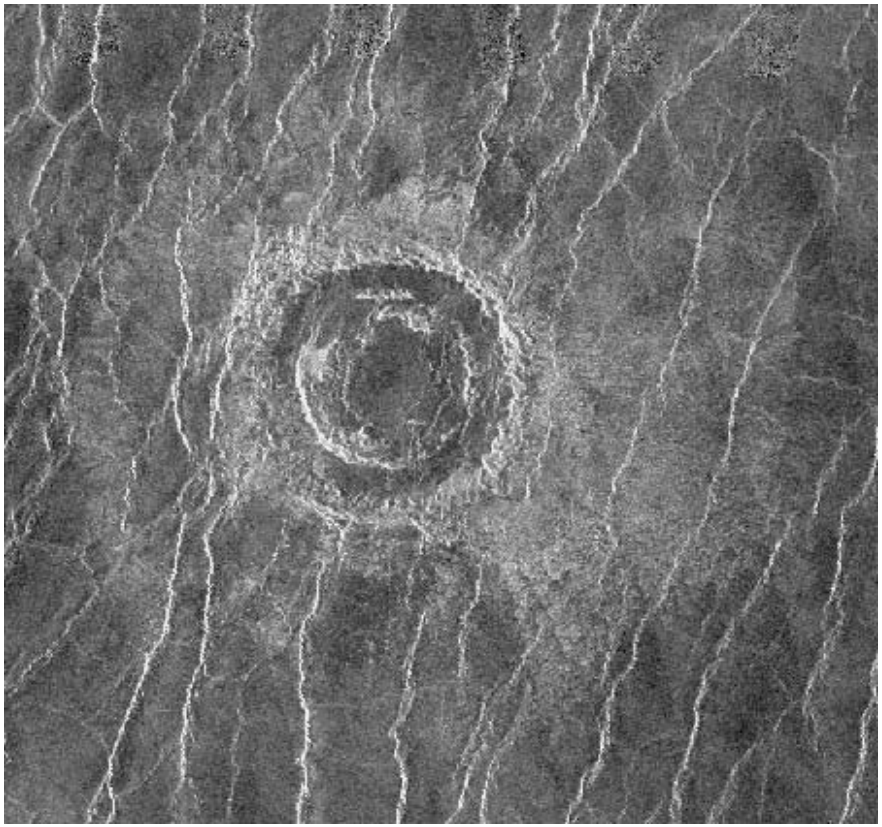

Radar image of Venus surface by NASA's Magellan spacecraft

Wrinkle ridges may have been formed by thermal stress caused by a sporadic enhancement of greenhouse effect (H_2O?) in the past.

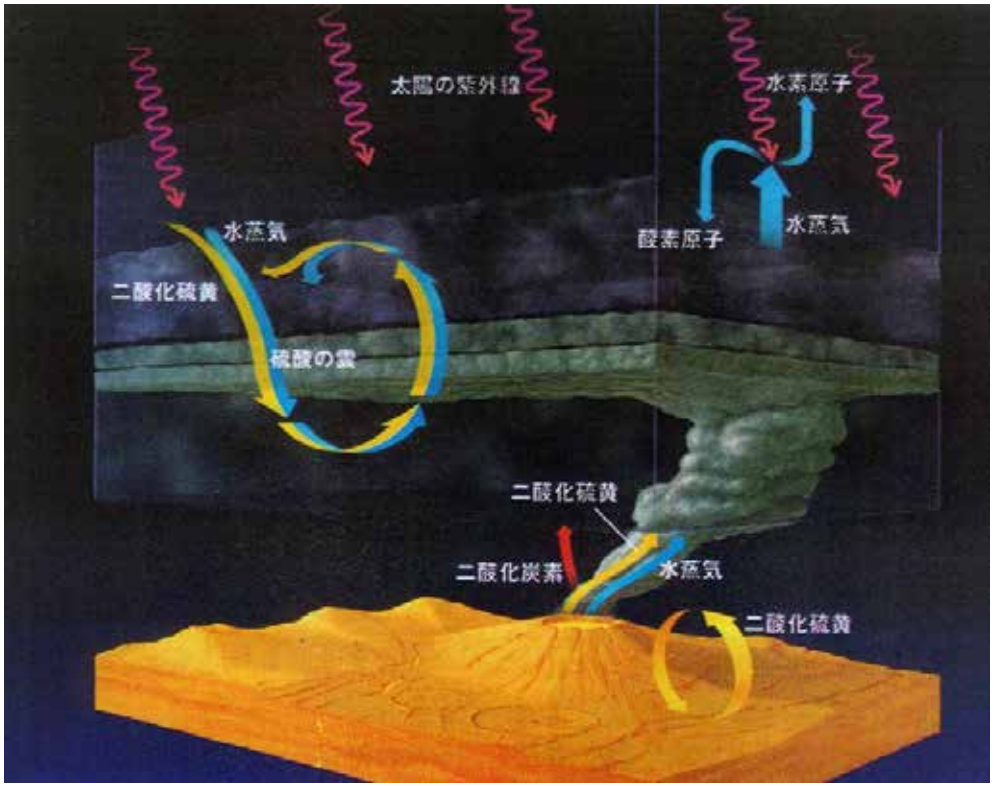

Recent Evolution of Climate on Venus (Bullock and Grinspoon 2001)

One-dimensional radiative-convective model coupled with cloud formation

H_2SO_4 cloud is produced from SO_2 and H_2O.
The abundances of SO_2 and H_2O change through volcanic eruption, surface reaction, and escape to space.

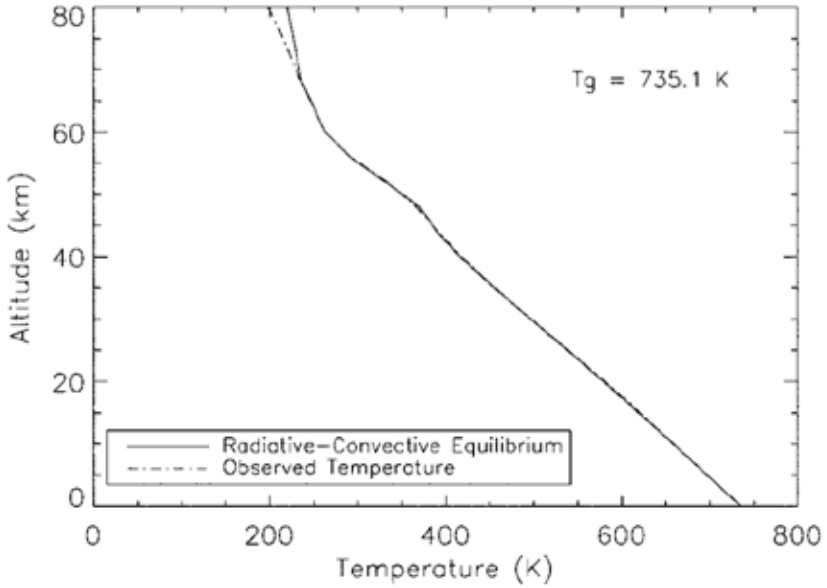

FIG. 2. Temperature profile calculated from the Venus radiative transfer model (solid line). For comparison, the Venus International Reference Atmosphere is plotted with a dashed line (Kliore *et al*. 1986).

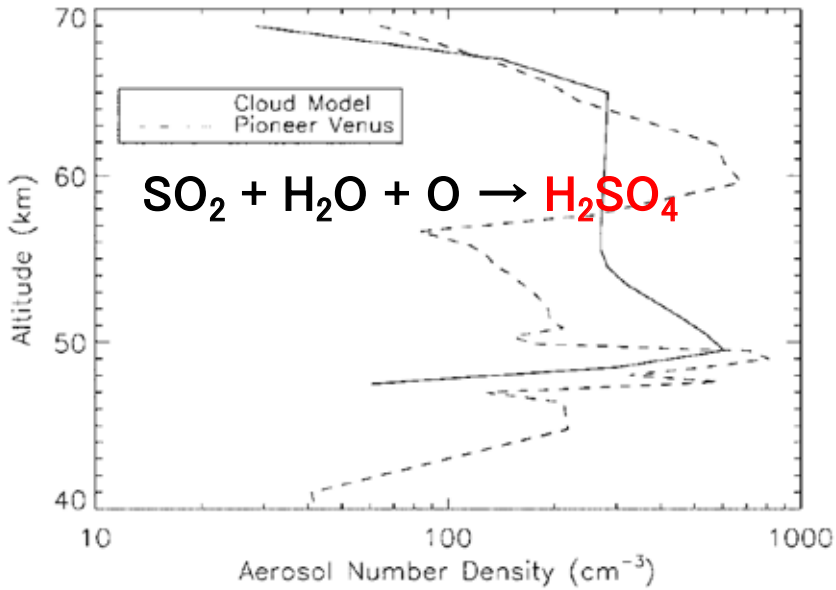

FIG. 5. Nominal cloud number densities as a function of altitude (solid line). Results for the real Venus cloud from the *Pioneer Venus* nephelometer are shown with the dashed line.

Temporal development

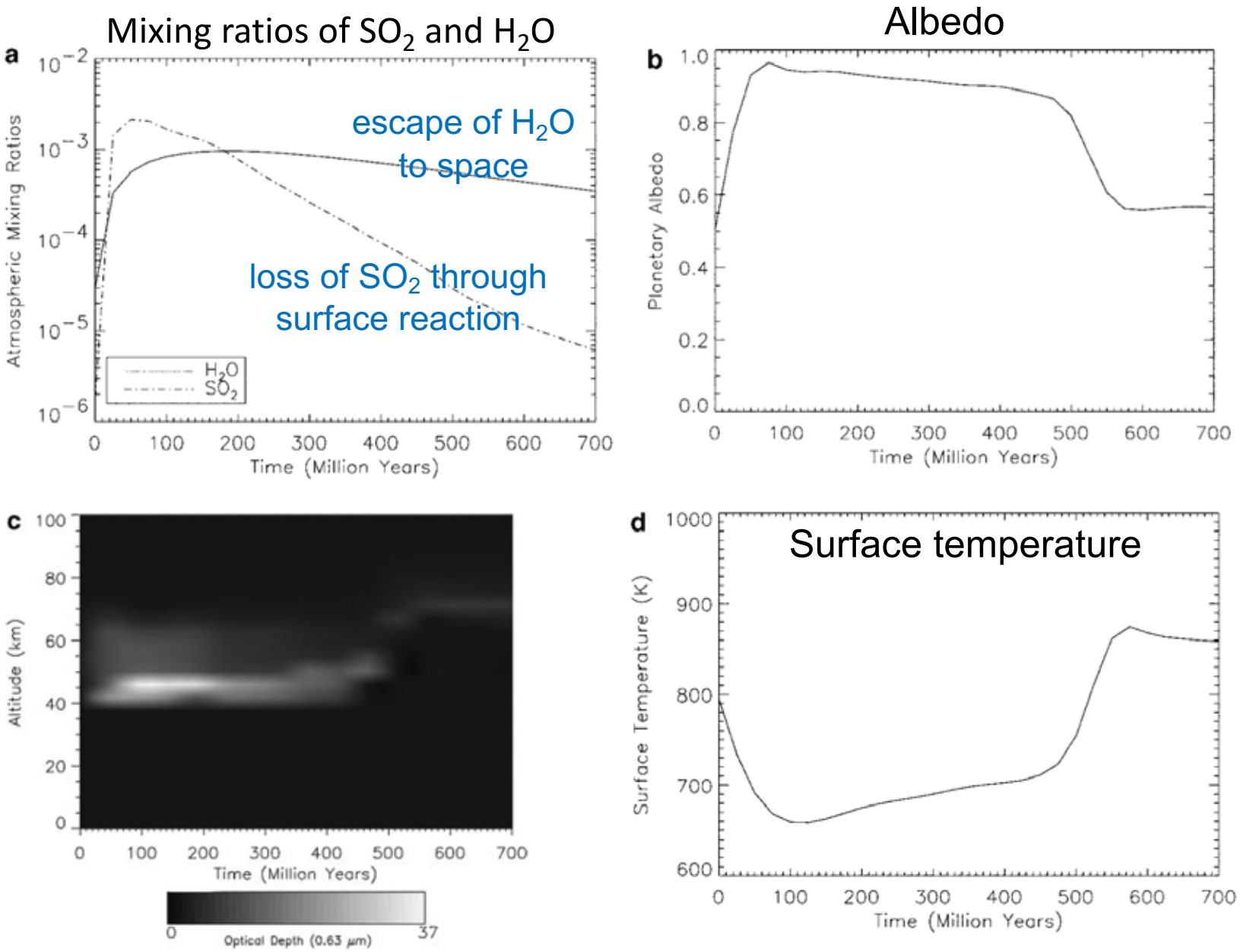

FIG. 10. Case 2: Rapid outgassing (100 Myr, 10 km), with exospheric escape (160 Myr) and SO_2 reactions with the surface. (a) is the evolution of atmospheric mixing ratios as a function of time. The solid line is for H_2O, dot–dashed line is for SO_2. (b) is the evolution of planetary albedo. (c) shows the evolution of cloud optical depths as a function of time. (d) shows the evolution of surface temperature as a function of time.

Variability of SO_2 above clouds

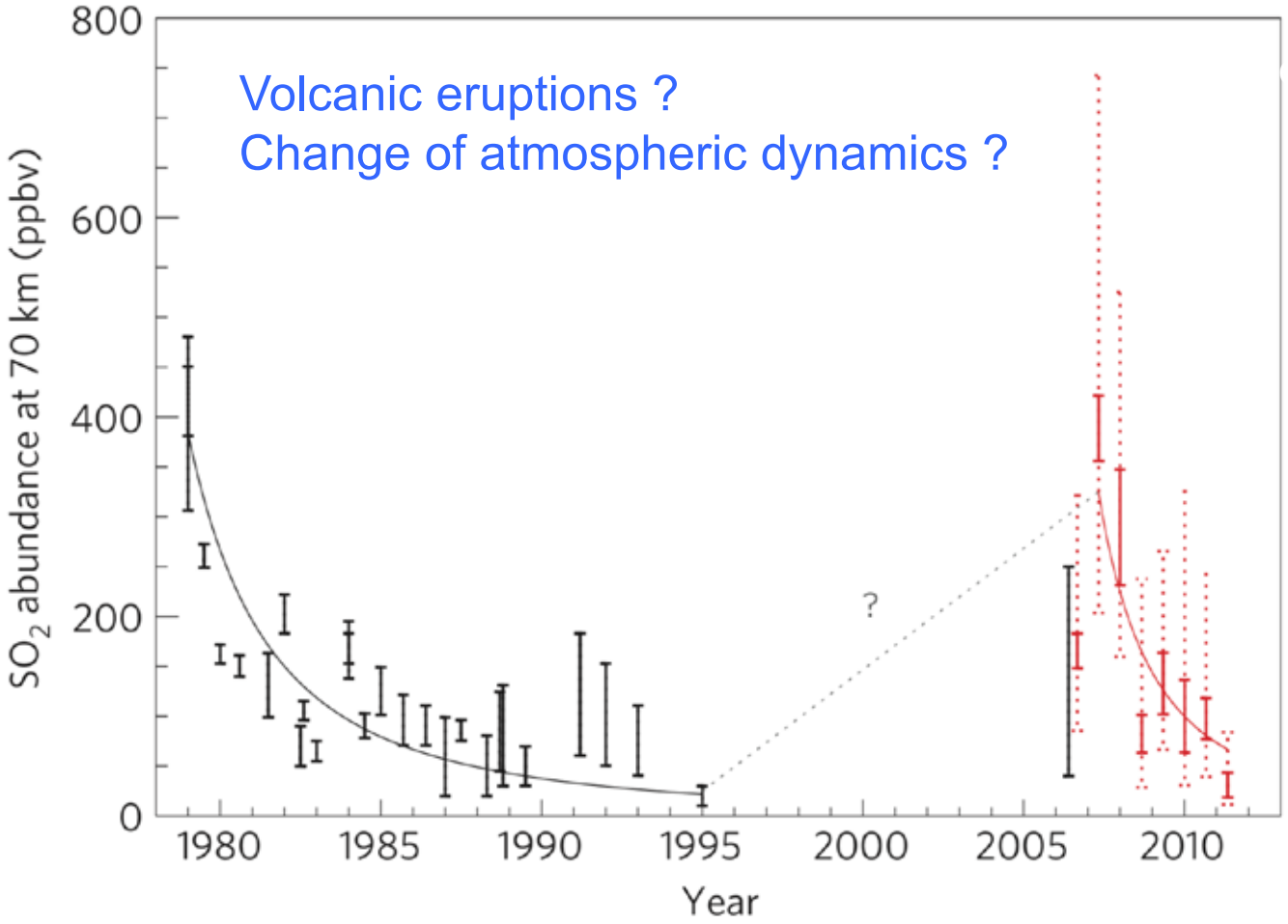

Marcq et al. (2013)

Figure 3 | More than thirty years of SO_2 measurements at Venus's cloud top. Black stands for previously published measurements[26]. Red stands for the 8-month moving average of the retrievals also shown in Fig. 1. Solid red error bars represent 1σ random uncertainty, and dotted red error bars represent measurement dispersion in each temporal bin.

Correlation between UV contrast and SO_2 density ? (Lee et al. 2015)

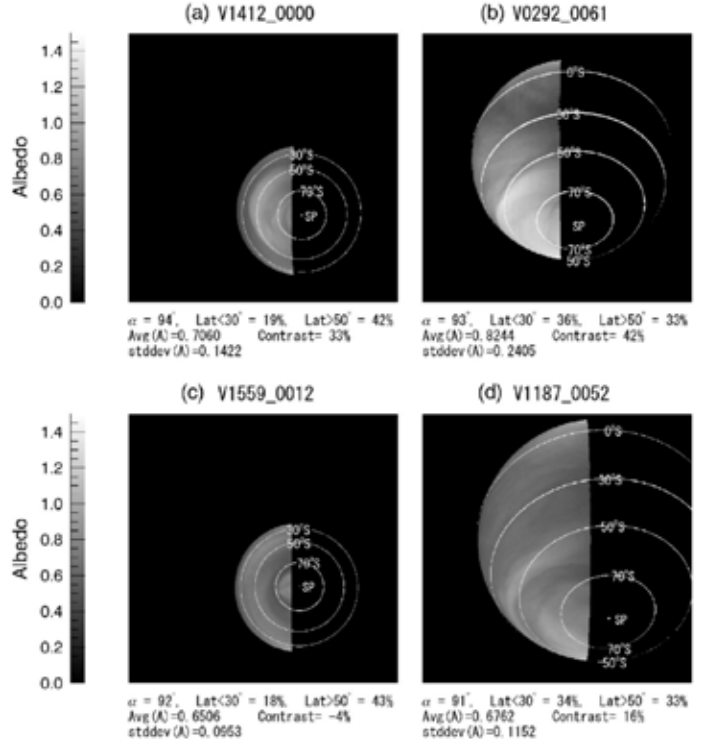

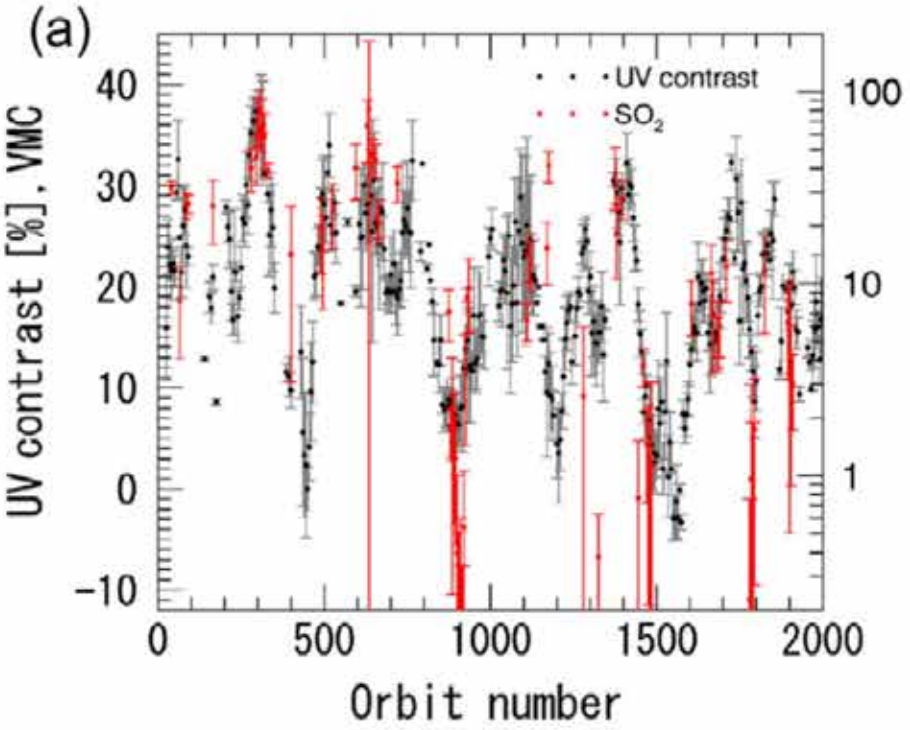

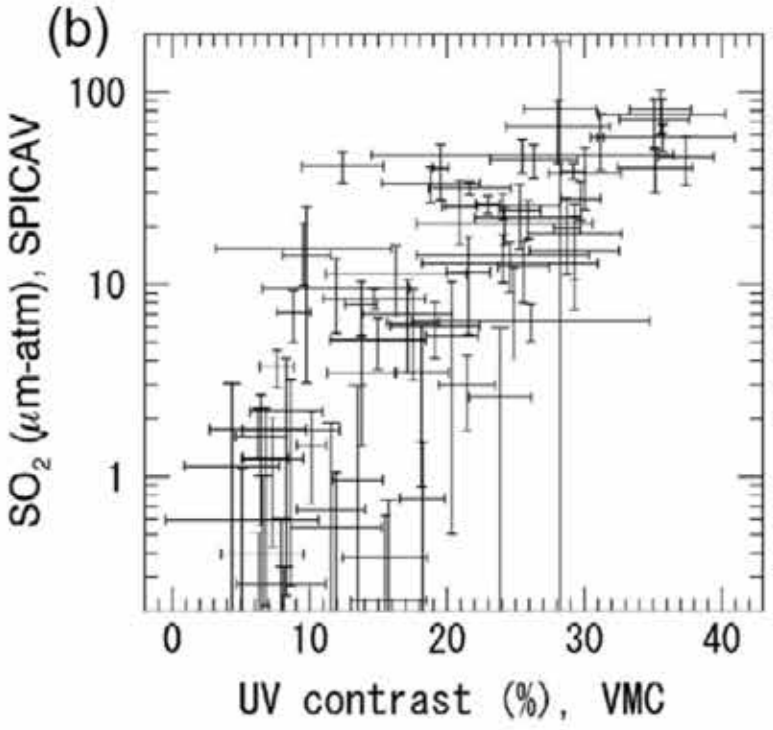

Long-term variations of the UV albedo of Venus (Lee et al. 2019)

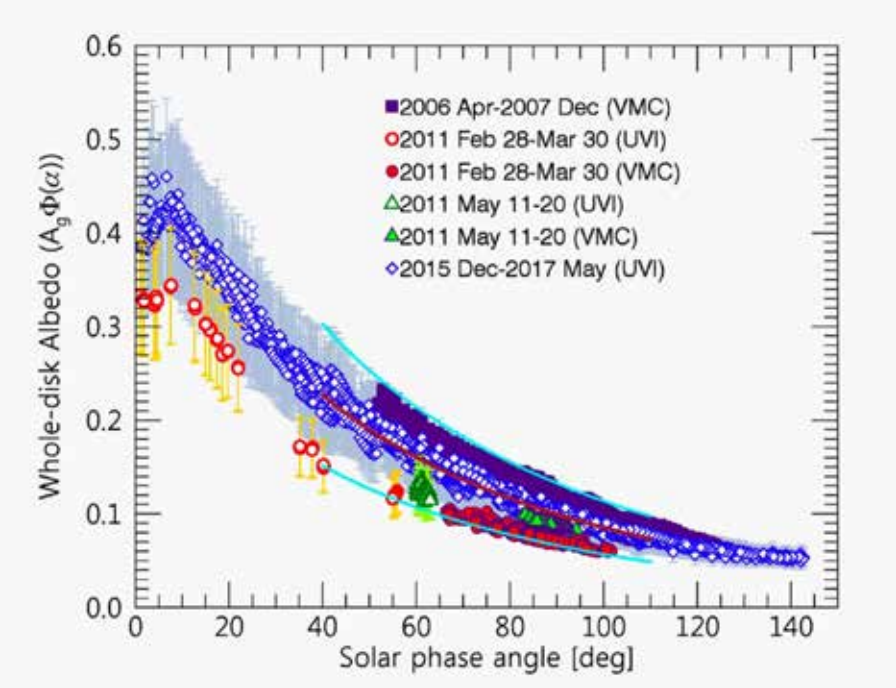

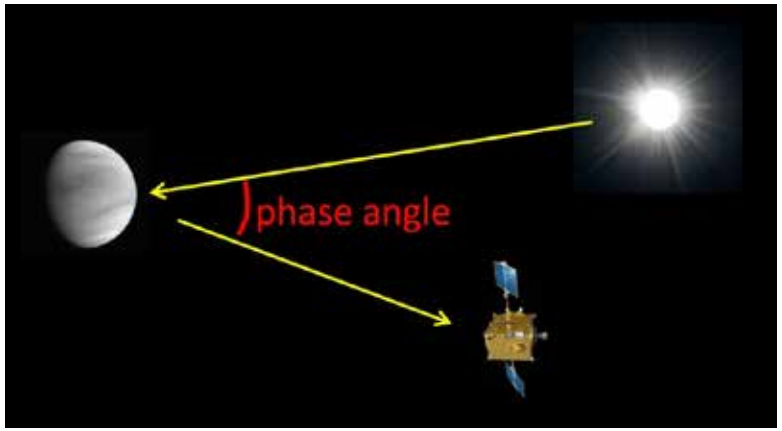

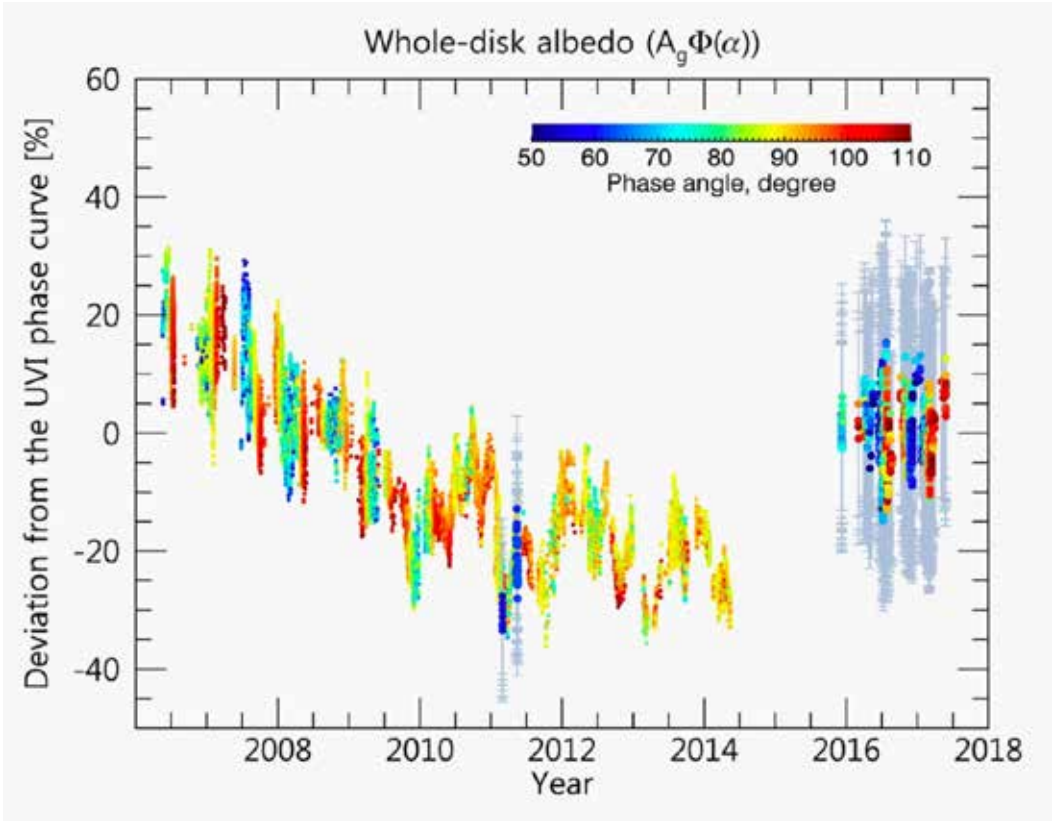

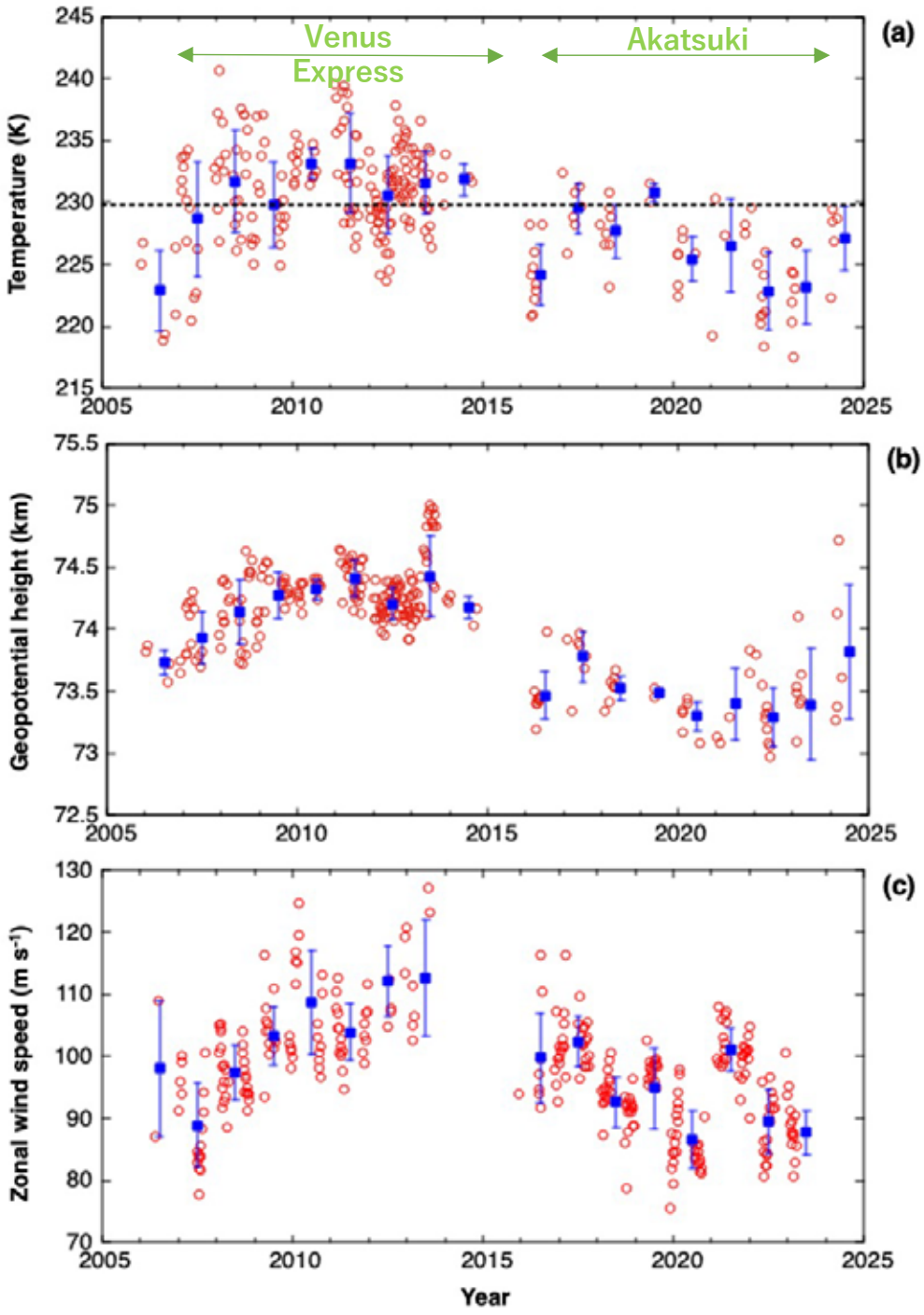

Temperature at the pressure level of 3.2×10^3 Pa (~70 km)

Geopotential height at the pressure level of 1.0×10^3 Pa (~75 km).

Zonal wind speed at cloud-top level obtained from Venus Express and Akatsuki UV cloud tracking

Ando et al. 2025

long-term variation of zonal wind in deep clouds
(Peralta et al. 2018)

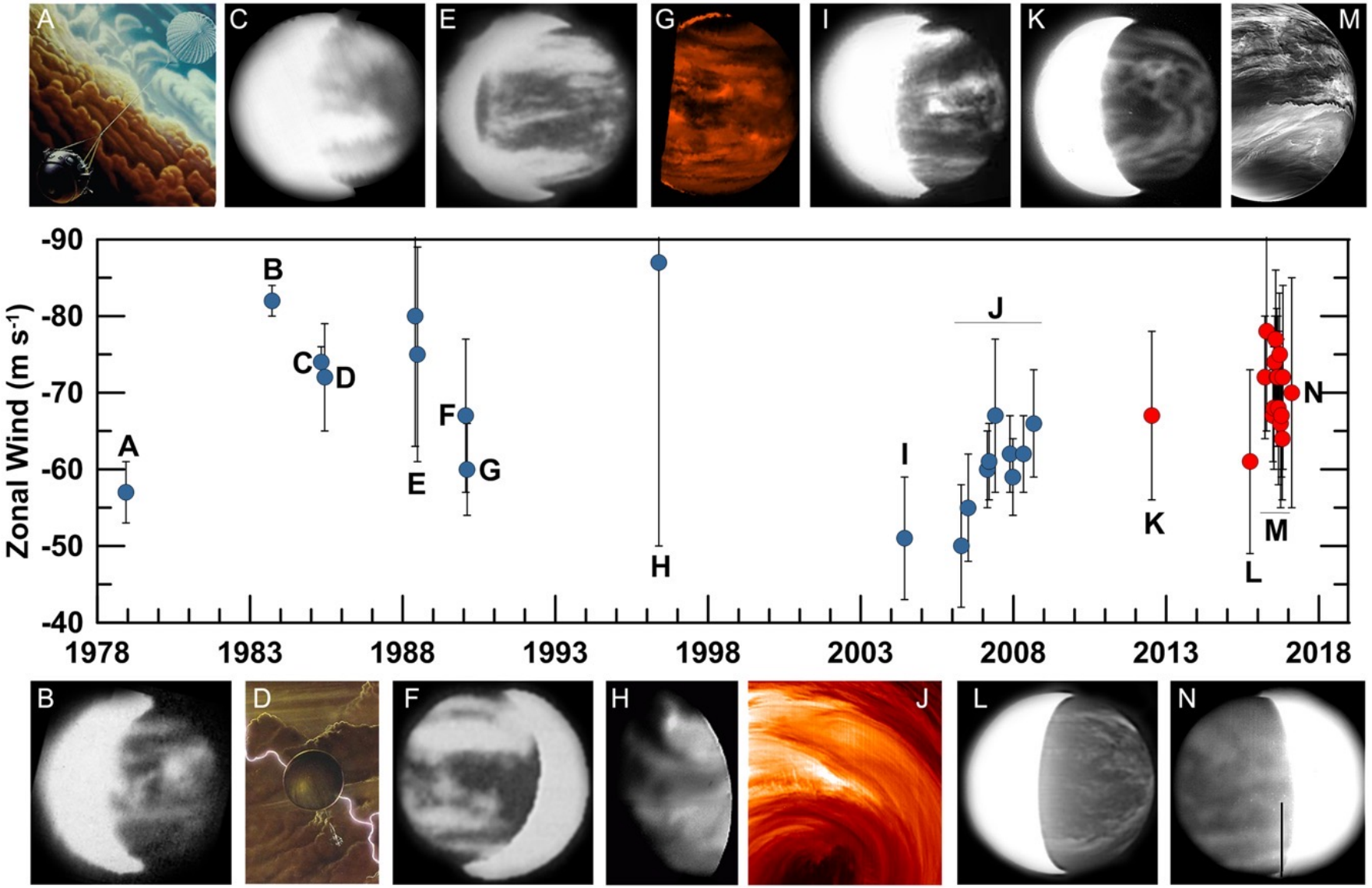

Radiative relaxation time

- Times cale of infrared cooling/solar heating
- The meridional overturning time is usually considered to be similar to the radiative relaxation time.

- Radiative relaxation time is longer for larger atmospheric heat capacities.
  - Mars : 3 Earth days
  - Earth : 100 Earth days
  - Venus : 50 Earth years

* The dynamical time scale of Venus's atmosphere can also be very long → Internal oscillation ?

Spontaneous oscillation of the atmosphere

- Earth : Quasi-biennial oscillation（QBO）

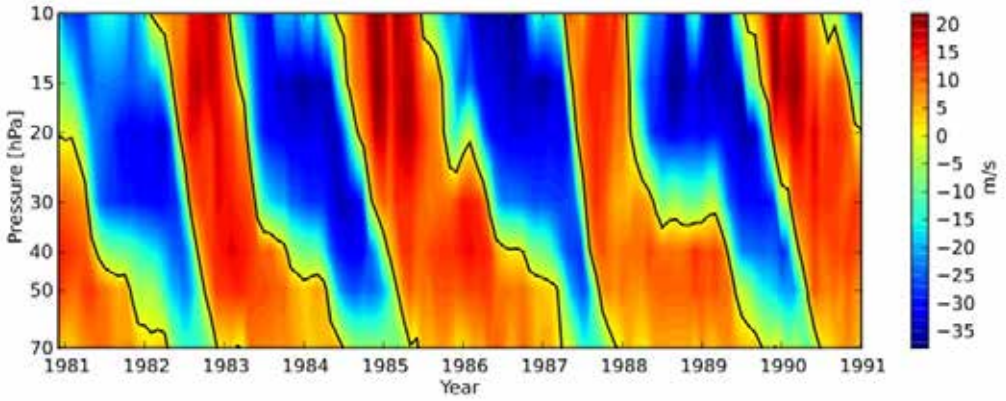

成層圏中下部(高度31～17km付近)の東西風速分布の断面図 (Wikipedia)

- システム内部の素過程の相互作用の手がかり

- 惑星では、木星の準4年振動（QQO）、火星のglobal dust stormの不定期発生、金星のスーパーローテーションの年々変動　など

Observations of exoplanets' atmospheres

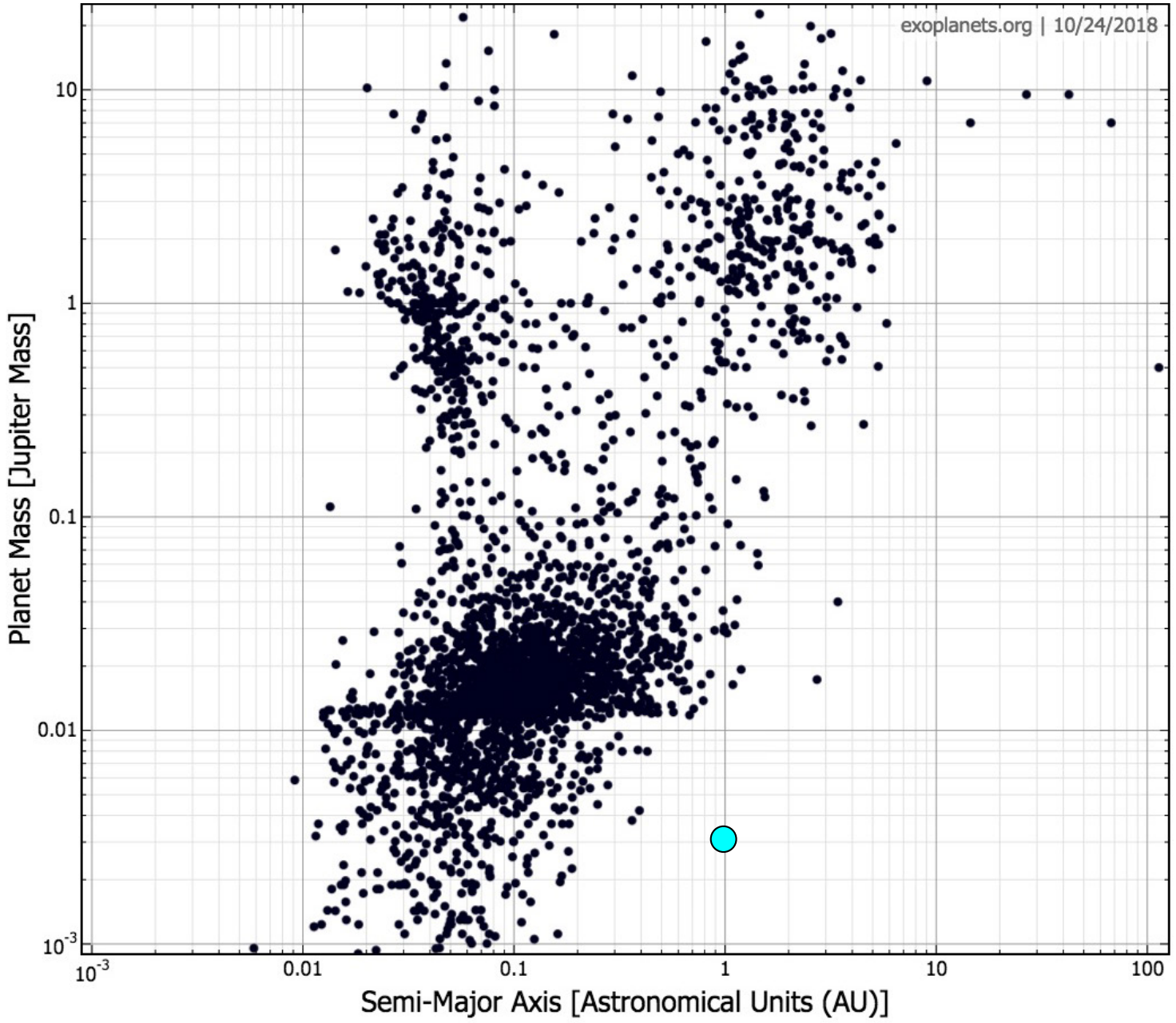

doi:10.1038/nature23266

Evans et al. (2017, Nature)

An ultrahot gas-giant exoplanet with a stratosphere

Thomas M. Evans[1], David K. Sing[1], Tiffany Kataria[2], Jayesh Goyal[1], Nikolay Nikolov[1], Hannah R. Wakeford[3], Drake Deming[4], Mark S. Marley[5], David S. Amundsen[6,7], Gilda E. Ballester[8], Joanna K. Barstow[9], Lotfi Ben-Jaffel[10], Vincent Bourrier[11], Lars A. Buchhave[12], Ofer Cohen[13], David Ehrenreich[11], Antonio García Muñoz[14], Gregory W. Henry[15], Heather Knutson[16], Panayotis Lavvas[17], Alain Lecavelier des Etangs[10], Nikole K. Lewis[18], Mercedes López-Morales[19], Avi M. Mandell[3], Jorge Sanz-Forcada[20], Pascal Tremblin[21] & Roxana Lupu[22]

- secondary eclipse of WASP-121b on 10 November 2016 using the Hubble Space Telescope (HST) Wide Field Camera 3 (WFC3)
- If upper layers are cooler than lower layers, molecular gases will produce absorption features in the planetary thermal spectrum. Conversely, if there is a stratosphere—where temperature increases with altitude—these molecular features will be observed in emission
- near-infrared thermal spectrum for the ultrahot gas giant WASP-121b, which has an equilibrium temperature of approximately 2,500 kelvin
- Water is resolved in emission, providing a detection of an exoplanet stratosphere

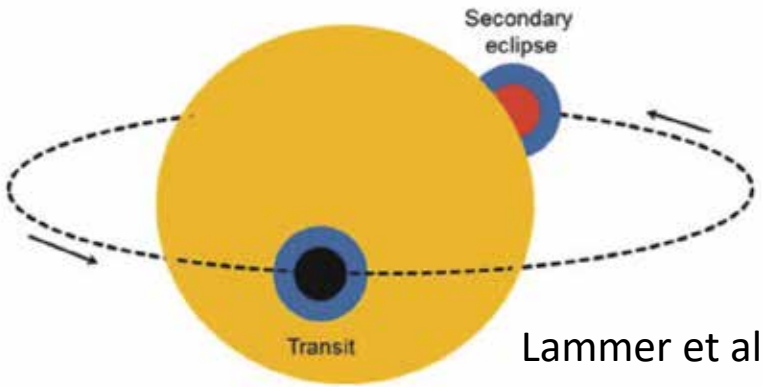

Lammer et al. (2013)

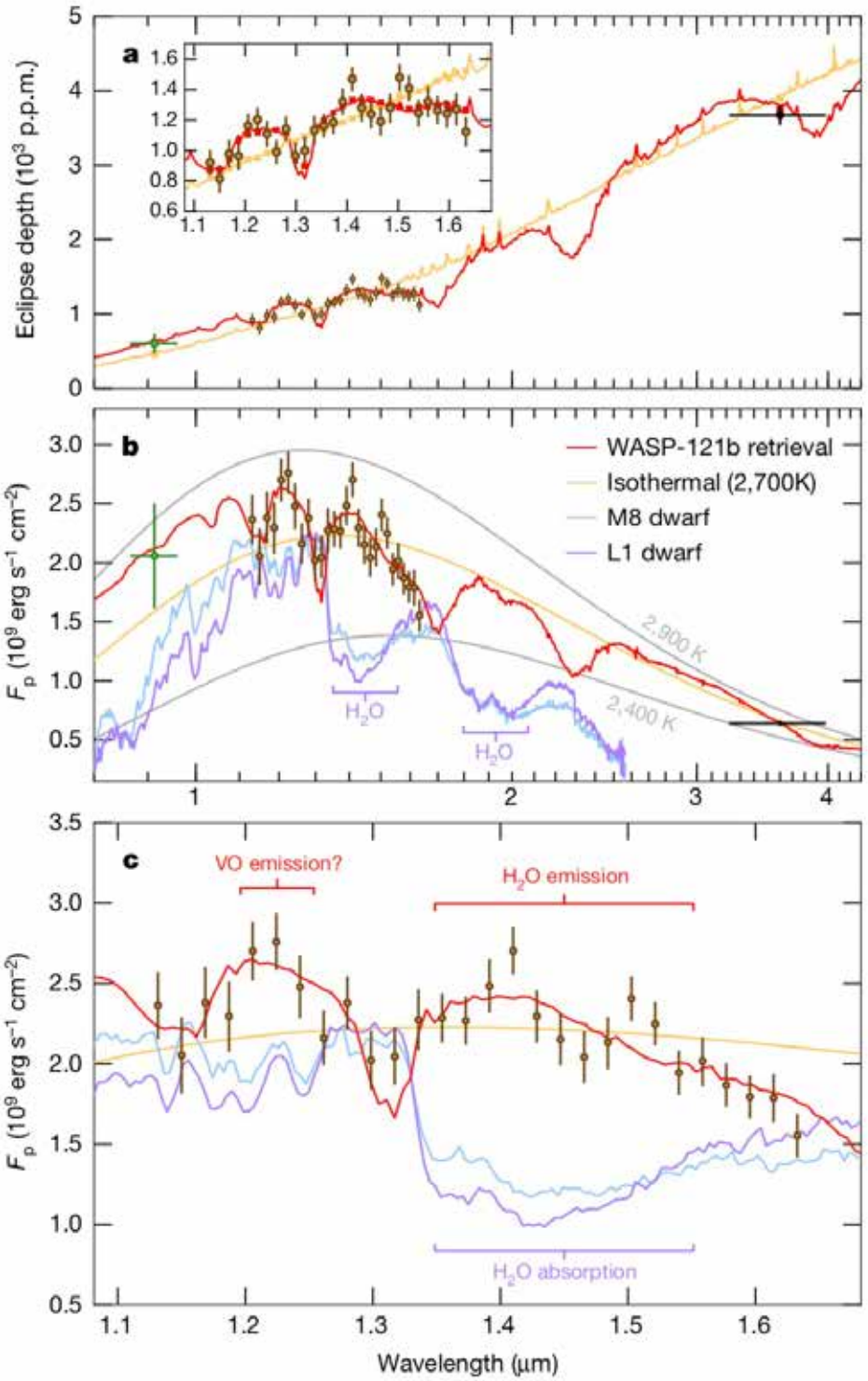

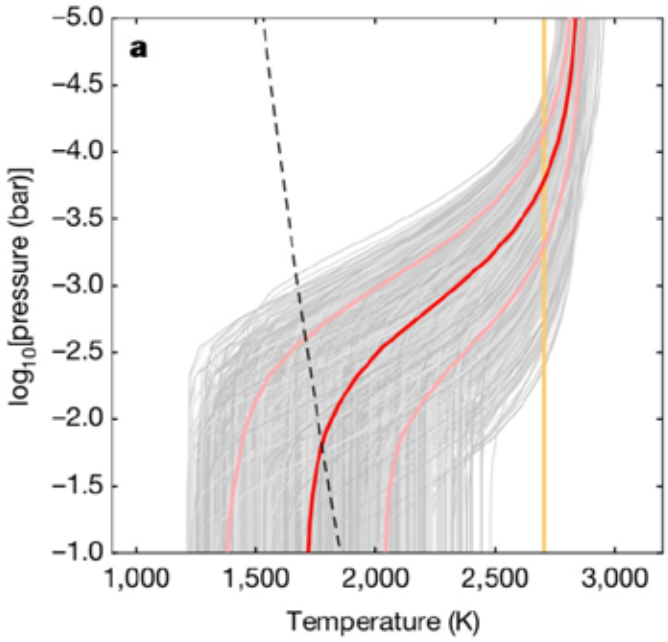

Figure 3 | Temperature–pressure profiles for WASP-121b. a, Grey lines show a random subset of *T*–*P* profiles sampled by the MCMC retrieval analysis. Red line shows the median temperature at each pressure level, and pink lines show ranges either side encompassing ±34% of the sampled profiles. Yellow line indicates the best-fit isothermal temperature of

A&A 577, A62 (2015)
DOI: 10.1051/0004-6361/201525729

Astronomy & Astrophysics

Spectrally resolved detection of sodium in the atmosphere of HD 189733b with the HARPS spectrograph*

A. Wyttenbach, D. Ehrenreich, C. Lovis, S. Udry, and F. Pepe

- high-resolution transit spectrum of HD 189733b in the region around the resonance doublet of Na I at 589 nm
- HARPS spectrograph (R = 115 000) at the ESO 3.6-m telescope
- blueshift corresponding to winds blowing at 8 $\pm$ 2 km s^{-1}

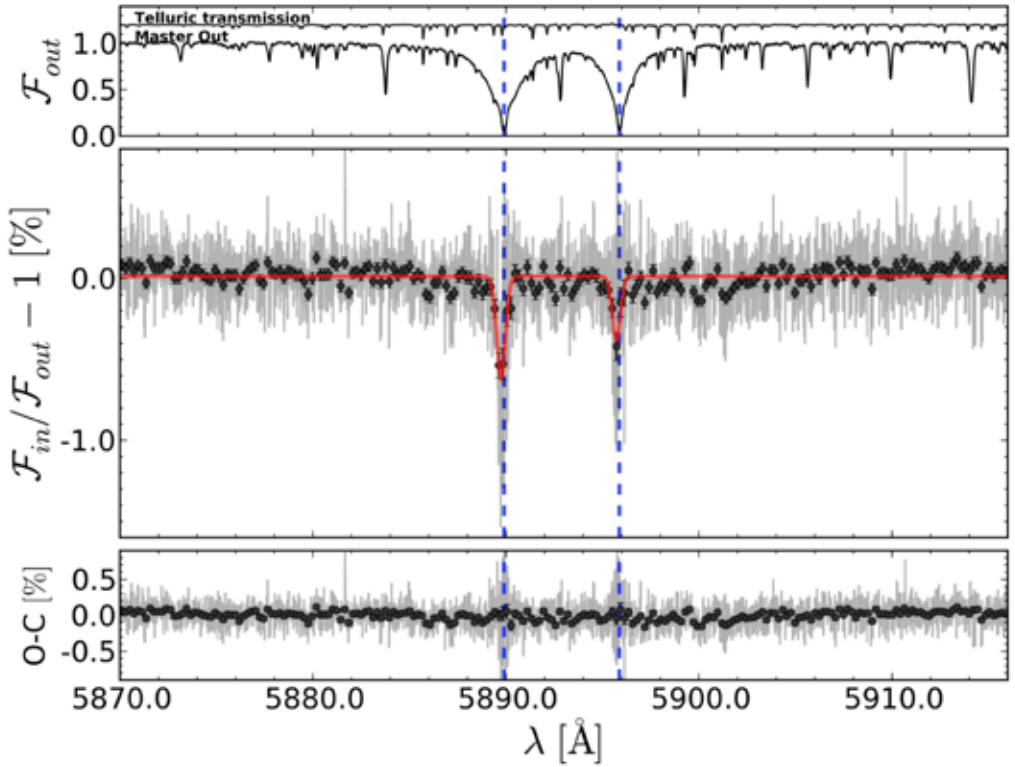

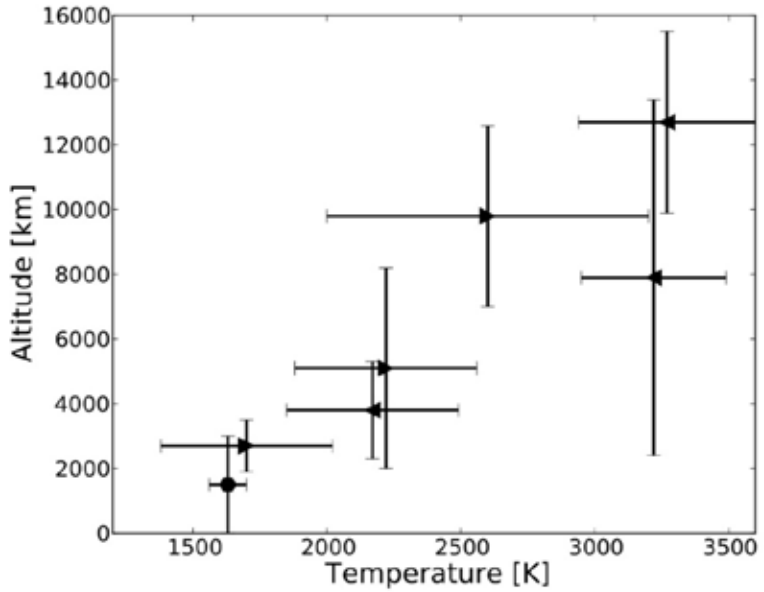

Fig. 9. Temperature profile obtained by our fitting process of η models to the transmission spectrum. The right and left triangle correspond to the Na I D1 and D2 lines. The diamond correspond to the wing shoulders. A temperature gradient of ~0.2 K km^{-1} is measured.

doi:10.1038/nature12888

Clouds in the atmosphere of the super-Earth exoplanet GJ 1214b

Kreidberg et al. (2014, Nature)

Laura Kreidberg[1], Jacob L. Bean[1], Jean-Michel Désert[2,3], Björn Benneke[4], Drake Deming[5], Kevin B. Stevenson[1], Sara Seager[4], Zachory Berta-Thompson[6,7], Andreas Seifahrt[1] & Derek Homeier[8]

- Transmission spectroscopy using Hubble Space Telescope
- We rule out cloud-free atmospheric models with compositions dominated by water, methane, carbon monoxide, nitrogen or carbon dioxide
- The planet's atmosphere must contain clouds

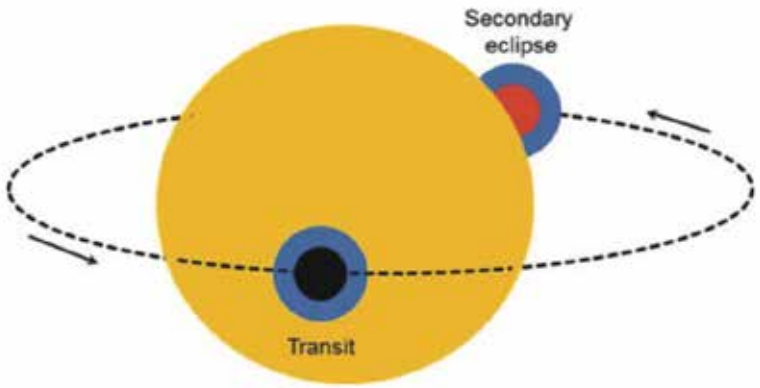

Lammer et al. (2013)

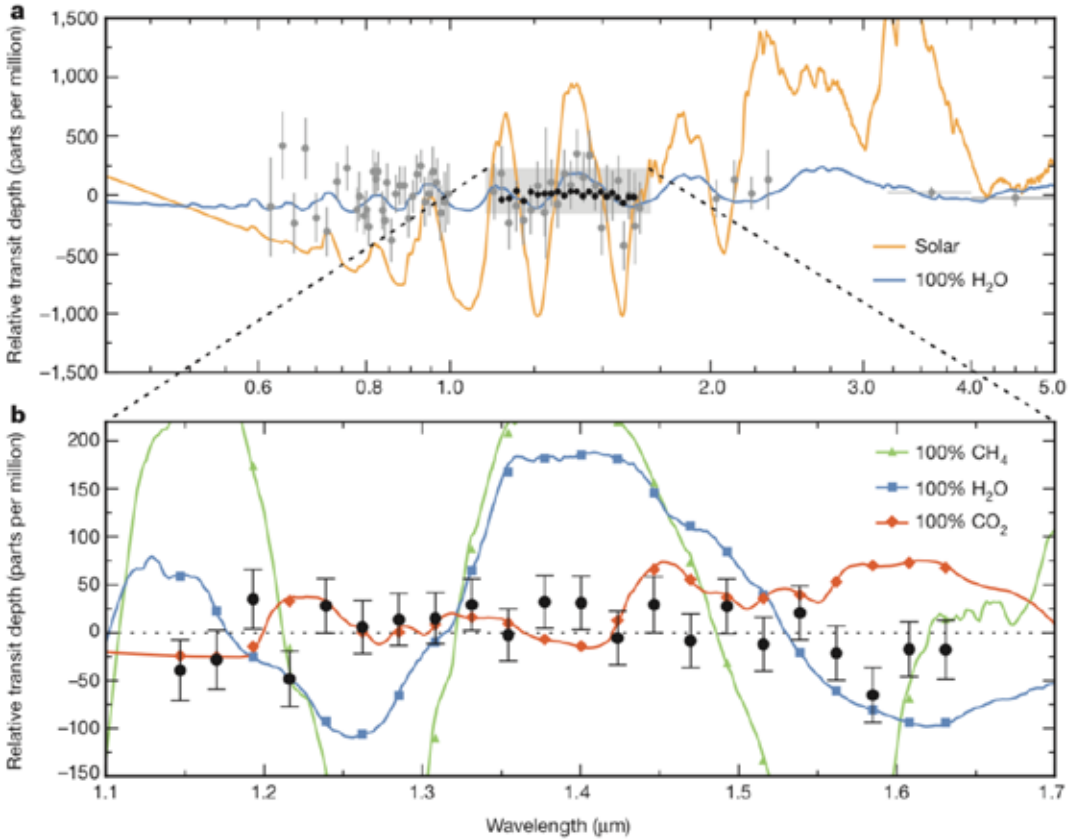

Meadows et al. (2018)
ASTROBIOLOGY, Vol 18

FIG. 6. Transit transmission spectra of potential planetary environments with different O_2 abundances for planet orbiting the M5.5V star Proxima Centauri (Meadows *et al.*, 2018). Illustrating spectral features that can help distinguish photosynthetic from abiotically generated O_2 in a planetary atmosphere. From top to bottom: self-consistent Earth-like atmosphere with 50% cloud cover (21% O_2); 10 bar abiotic O_2 (95% O_2) atmosphere produced by early ocean loss with ocean remaining (purple) and desiccated (orange); 1 bar desiccated CO_2/CO/O_2 atmosphere that has reached a kinetic–photochemical equilibrium between the photolysis rate of CO_2 and kinetics-limited recombination (15% O_2). Effective atmospheric radius in kilometers is on the left *y* axes and transit depth is shown on the right *y* axes. The photosynthetic source for O_2 in the Earth-like case is made more likely by the presence of O_2/O_3, water, and methane. High O_2 cases with and without water are distinguished by the presence of O_4, and the behavior of the 0.5–0.7 μm Chappuis band that is sensitive to tropospheric O_3, which is more abundant in the desiccated case. The desiccated chemical equilibrium atmosphere is easily distinguished by its high levels of CO.

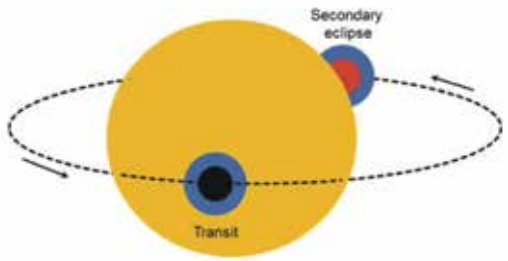

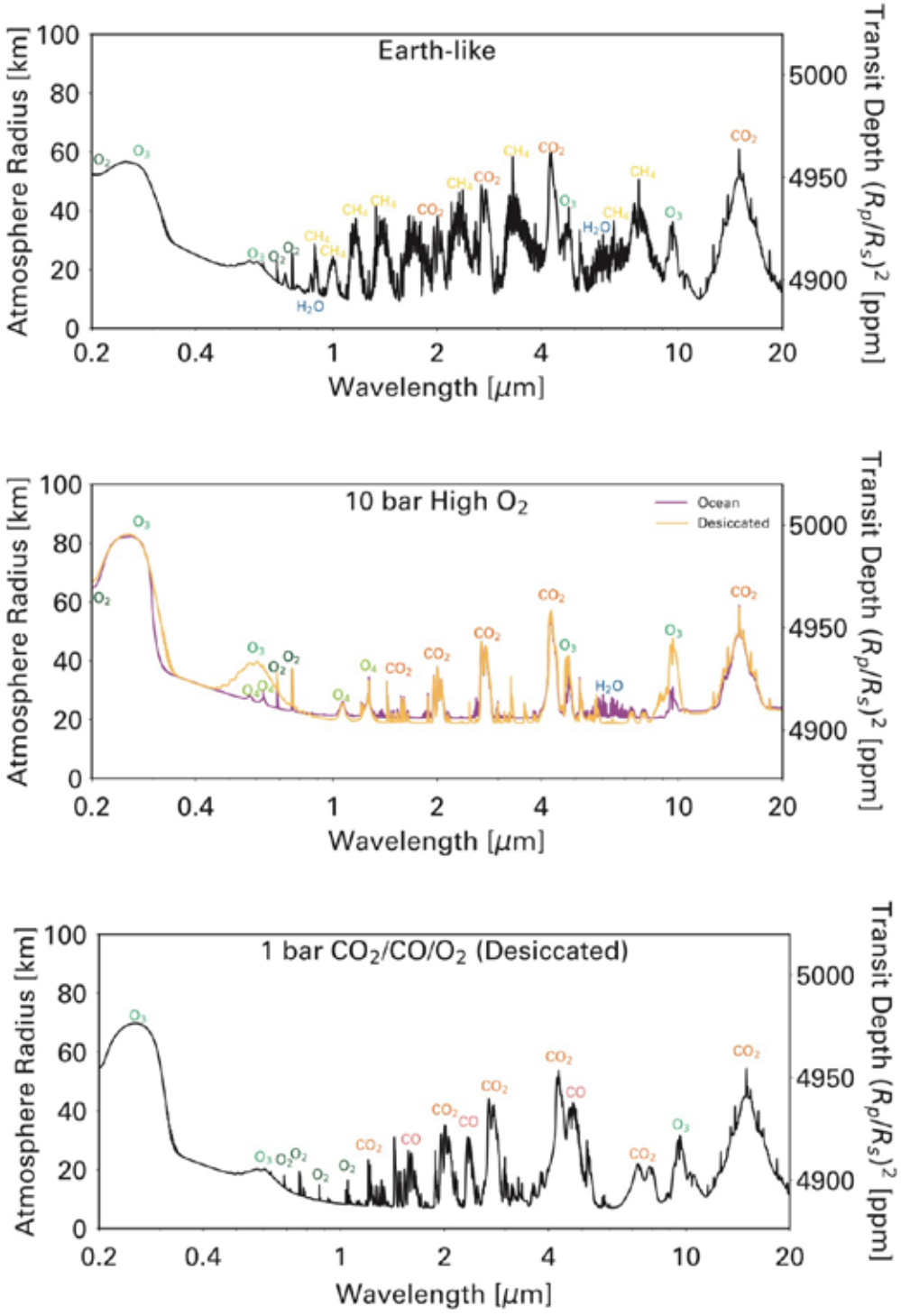

A map of the day-night contrast of the extrasolar planet HD 189733b (Knutson et al. 2007)

A minimum brightness temperature of 973 +/- 33 K and a maximum brightness temperature of 1212 +/- 11 K at a wavelength of 8 microns, indicating that energy from the irradiated dayside is efficiently redistributed throughout the atmosphere

Observed phase variation for HD 189733b, with transit and secondary eclipse visible.

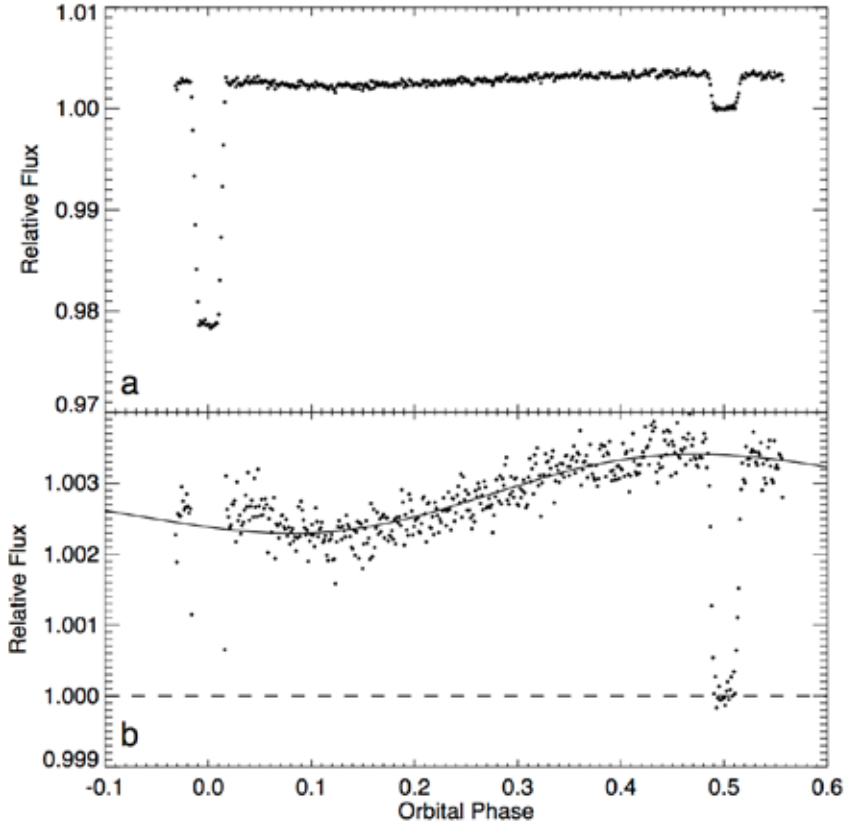

Brightness estimates for 12 longitudinal strips on the surface of the planet